



The Effect of South American Biomass Burning Aerosol Emissions on the Regional Climate

Gillian D. Thornhill¹, Claire L. Ryder¹, Eleanor J. Highwood¹, Len C. Shaffrey^{1,3}, and Ben T. Johnson²

¹Department of Meteorology, University of Reading, Reading, UK

²Met Office, Exeter, UK

³National Centre for Atmospheric Science, University of Reading, UK

Correspondence to: G. D. Thornhill (g.thornhill@reading.ac.uk)

Abstract. The impact of biomass burning aerosol (BBA) on the regional climate in South America is assessed using 30 year simulations with a global atmosphere-only configuration of the Met Office Unified Model. We compare two simulations of high and low emissions of biomass burning aerosol based on realistic interannual variability. The aerosol scheme in the model has hygroscopic growth and optical properties for BBA informed by recent observations, including those from the recent South American Biomass Burning Analysis (SAMBBA) intensive aircraft observations made during September 2012. We find that the difference in the September (peak biomass emissions month) BBA optical depth between a simulation with high emissions and a simulation with low emissions corresponds well to the difference in the BBA emissions between the two simulations, with a 70 % reduction from high to low emissions for both the BBA emissions and the BB AOD in the region with maximum emissions (defined by a box of extent 5-25° S, 40-70° W, used for calculating mean values given below). The cloud cover at all altitudes in the region of greatest BBA difference is reduced as a result of the semi-direct effect, by heating of the atmosphere by the BBA and changes in the atmospheric stability and surface fluxes. Within the BBA layer the cloud is reduced by burn-off, while the higher cloud changes appear to be responding to stability changes. The boundary layer is reduced in height and stabilised by increased BBA, resulting in reduced deep convection and reduced cloud cover at heights of 9-14km, above the layer of BBA. Despite the decrease in cloud fraction, September downwelling clear-sky and all-sky shortwave radiation at the surface is reduced for higher emissions (by 13.79 W/m² clear-sky, 7.42 W/m² all-sky) whilst the upwelling shortwave radiation at the top of atmosphere is increased in clear sky by 3.33 W/m², but decreased by -1.32 W/m² when cloud changes are included. Shortwave heating rates increase in the aerosol layer by 18% in the high emissions case. The mean surface temperature is reduced by 0.14 °C and mean precipitation is reduced by 15% in the peak biomass region due to both changes in cloud cover and cloud microphysical properties. If the increase in BBA occurs in a particularly dry year, the resulting reduction in precipitation may exacerbate the drought. The position of the South Atlantic High pressure is slightly altered by the presence of increased BBA and the strength of the southward low level jet to the east of the Andes is increased. There is some evidence that some impacts of increased BBA persist through the transition into the monsoon, particularly in precipitation, but the differences are only statistically significant in some small regions in November. This study therefore provides an insight into how variability in deforestation and biomass burning emissions may contribute to the South American climate, and consequently on the possible impacts of future changes in BBA emissions.



1 Introduction

Land management practices in South America designed to increase available land for agriculture and pasture and increasing urbanization have resulted in deforestation altering an estimated 18% of the original forest area (Artaxo et al., 2013). The emissions from fires tend to be largest where there is rapid deforestation (e.g. south-east Amazonia), lowest in the tropical forests in central Amazonia where the density of the forest canopy and larger amounts of moisture generally prevent fires, and areas where the fires occur in already cleared agricultural and pastoral land tend to have lower fuel loads and result in reduced fire emission per unit area compared to areas of rapid deforestation (Reddington et al., 2015; DeFries et al., 2008).

The biomass burning aerosols (BBA) absorb and scatter radiation, and affect the surface fluxes and atmospheric stability. BBA also increase the concentration of cloud condensation nuclei (CCN) affecting the formation and lifetime of clouds (Koren et al., 2008; Sena et al., 2013; Koch and Del Genio, 2010). They consist largely of carbonaceous material, with a relatively low single scattering albedo (SSA) indicating they are more absorbing than e.g. sulphate aerosols. There is a direct effect on the radiative budget from both scattering and absorption (Charlson et al., 1992), and the absorption results in atmospheric heating which, together with the reduced solar radiation reaching the surface, changes the stability of the atmosphere. Heating of the atmosphere where aerosols and clouds are co-located (in altitude) is predicted to result in cloud cover changes as cloud 'burns off' or is prevented from forming due to the stabilisation of the atmospheric profile. This process has been termed the semi-direct effect (Hansen et al., 1997; Koren et al., 2008); although other studies have pointed out that the semi-direct effect could have the opposite tendency, for instance if increased atmospheric stability favors the persistence of stratocumulus (Johnson et al., 2004). The overall aerosol-cloud interaction is however complex, with the semi-direct effect depending on the relative heights of the aerosol and the clouds, the type of cloud and the regional dynamics e.g. convergent or divergent flow (Koch and Del Genio, 2010). The particles of smoke are also predicted to act as cloud condensation nuclei, (Spracklen et al., 2011), changing the size and number of cloud droplets resulting in changes to the reflectivity and lifetime of the clouds, referred to as the indirect effect (Twomey, 1974; Albrecht, 1989). Effects of BBA on convection and cloud formation characteristics can result in changes in precipitation (Gonçalves et al., 2015), which in turn will change hydrological processes, (Koren et al., 2004). Furthermore changes in the proportions of direct and diffuse radiation at the surface will affect photosynthesis and net primary productivity (Rap et al., 2015). Koren et al. (2008) investigated the effect of BBA on cloud formation and lifetime and suggested that the stabilisation of the lower atmosphere, and the reduction in fluxes from the surface can inhibit the formation of high and deep convective clouds, despite the possible destabilisation of the higher atmosphere due to the increased heating of the atmosphere at lower levels. This effect is dependent on the initial cloud cover fraction however, as a lower initial cloud cover permits more solar absorption and increases the aerosol heating effects. The BB AOD is also a factor, with the suggestion that at low(high) BB AOD the indirect effect is more(less) important than the semi-direct effect (Ten Hoeve et al., 2012).

Assessing the relative importance of these various effects is crucial to understanding the overall impact of BBA on the regional climate, but there is some uncertainty in how to treat and describe aerosol properties in climate models that can affect the results of such studies. Our approach uses new observations of aerosol optical properties, and compares two different scenarios, a high BBA emission experiment with a low BBA emission experiment, so that we are considering changes due to



decadal time scale variability in emissions (rather than a comparison of the regional climate with BBA to one without BBA). This provides some insight into how changes in deforestation practices and the resulting changes in the characteristics of the BBA over time might affect the regional climate.

The climate of S. America shows considerable variability, due to its large latitudinal extent (12° N to 53° S) covering tropical, sub-tropical and extra-tropical climate zones. The Andes also produce large east-west variation, compounded by the change in the east-west width of the continent and the differences between the temperatures of the oceans, with the south-western Atlantic being warm, and the south-eastern Pacific being cool (Garreaud et al., 2009). In the tropics the Intertropical Convergence Zone corresponds to an east-west belt of low pressure and low-level convergence of the trade winds, resulting in an area of high annual mean precipitation which is largely produced by deep convective clouds. The annual precipitation shows a seasonal cycle, with austral winter (JJA) maximum rainfall in the north of the continent. Towards the end of October the convection shifts southwards, so that the austral summer is characterised by heavy precipitation from the southern Amazon basin to northern Argentina. During the austral autumn (MAM) the maximum precipitation moves back to the north. This seasonal pattern is considered by some to be monsoonal (Vera et al., 2006; Marengo et al., 2012), although it does not exhibit the reversal in low-level winds seen in other monsoon systems. The S. American monsoon generally has an onset in October, but the exact timing is variable, and geographically dependent, with an extension of the rainy area in the northwest of Amazonia down to southern Amazonia (Zhang et al., 2009). Generally there is an increase in precipitation from the NW to the SE from central America to the SE Amazon area, with the largest changes in the central Amazon area. Changes in the surface fluxes, with increases in surface radiation and sensible and latent heat flux are considered to be initiators of the monsoon. As the monsoon progresses, surface (sea level) pressure is expected to reduce over the S. Atlantic, while the sub-tropical high in the S. Atlantic is displaced eastwards and weakens (Marengo et al., 2012). Increased convection moves from down from the NW to central Amazonia and Brazil, while the circulation pattern at 850 hPa changes from northerlies to northwesterlies (Raia and Cavalcanti, 2008) in the SW part of Amazonia, and in E. Brazil from easterlies to northeasterlies following the displacement of the S. Atlantic high. Close to the mouth of the Amazon large scale northerly anomalies, and the reduction of the zonal component of the trade winds are expected as part of the transition to the monsoon (Marengo et al., 2001).

The South American Biomass Burning Analysis (SAMBBA) project was designed to use ground-based and aircraft observations of S. American biomass burning aerosols to investigate their impact on climate. It involved a consortium of international institutions, led by the UK Met Office, and the National Institute for Space Research (INPE) Brazil, in partnership with the University of Sao Paulo, and seven universities in the UK (Exeter University, Leeds University, Manchester University, University of Reading, University of East Anglia, University of York, King's College London). The observational flights were conducted in September 2012 over the Amazonian region and were coordinated with ground measurements (Allan et al., 2014; Brito et al., 2014; Marengo et al., 2016). The flights were designed to measure aerosol properties, the atmospheric chemistry, and the clouds, meteorology and radiation budget over Amazonia. The modelling presented here is part of the complementary effort to use the flight campaign observations results to refine BBA properties in global models and to ascertain the effects of these aerosols on regional climate.



In this article we test the sensitivity of the (regional) South American climate to realistic high and low BBA emission scenarios using aerosol properties constrained by aircraft campaign measurements. The main biomass burning months are August and September, so the results discussed in this paper focus on the changes in climate in September where the effects of the BBA on the regional climate are likely to be greatest, with a particular emphasis on cloud changes, the semi-direct effect, and changes in atmospheric stability which impact cloud changes. Finally, we also briefly examine the influence of changing emissions of BBA on the S. American monsoon onset. Section 2 describes the methodology and model setup, Section 3 describes the results for the September biomass burning season, Section 4 focuses on the impact on the monsoon, and Section 5 discusses the results and their significance.

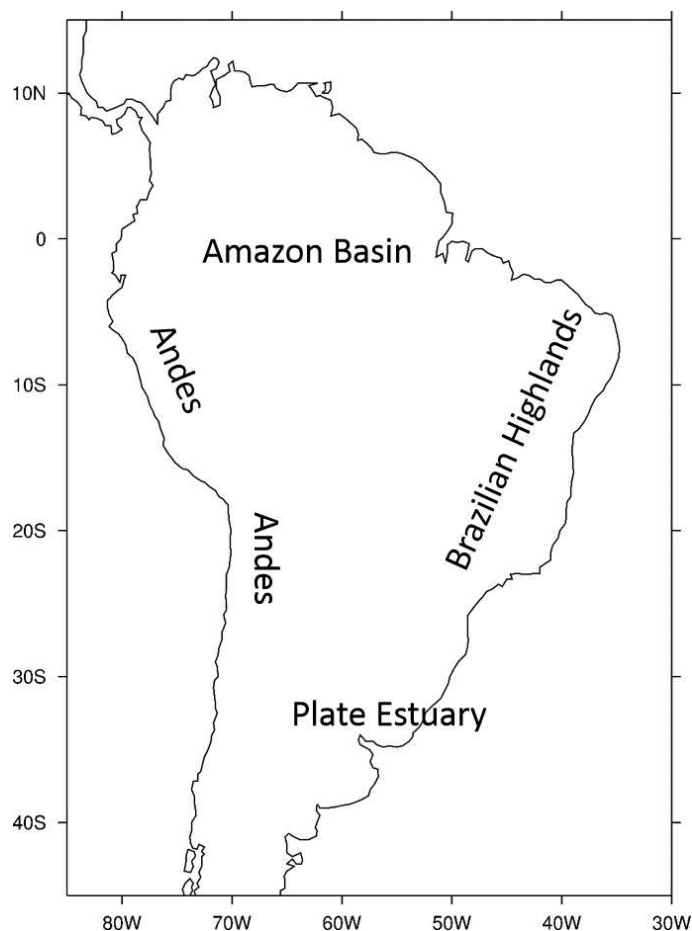


Figure 1. Map of S. America with features referred to in the text marked.



2 Methods

2.1 Model Setup

Global climate model simulations were performed with the Met Office Unified Model HadGEM3 GA3 (Hewitt et al., 2011) at a resolution of N96 (1.25 degrees by 1.875 degrees) with 85 vertical levels. Simulations were run over 30 years, with a spin up period of one year. Sea surface temperatures and sea ice were prescribed using data from HadISST (Rayner et al., 2003) using monthly means over 1997-2011. The cloud scheme used was the PC2 scheme (Wilson et al., 2008a, b). Monthly emission periodic climatologies for non-BBA are used, including the 2-D sulphur cycle, black carbon and organic carbon from fossil fuel burning, from the CMIP5 dataset (Lamarque et al., 2010) with monthly means representing 2000-2010. Biogenic secondary organic aerosols are represented by an AOD climatology. The atmosphere was free running. Aerosols were simulated by the Coupled Large-scale Aerosol Scheme for Simulations in Climate Models (CLASSIC), a mass-based ('bulk') aerosol scheme representing sulfate, fossil-fuel soot (black carbon), fossil-fuel organic carbon, biomass burning aerosol, sea salt and mineral dust aerosol species, where the physical and optical properties of each are specified, and are externally mixed. A full description is given in the appendix of Bellouin et al. (2011), and Johnson et al. (2016) provide a detailed description of the BBA scheme. The BBA scheme was originally introduced for HadGEM1 (Davidson et al., 2004) and soon revised (Jones et al., 2005) to use updated BBA properties based on the SAFARI-2000 aircraft field observations from Southern Africa (Haywood et al., 2003; Abel et al., 2003). BBA is represented as a single species (rather than as separate BC and OC components) with mass emitted into a fresh mode, and subsequently converted into a hygroscopic aged mode with an e-folding timescale of 6 h represented by an increase in mass by a factor of 1.62 (Abel et al., 2003). Since OC and BC are assumed to be internally mixed in the model, this increase in mass represents an increase in the mass of OC in BBA as the aerosol ages chemically and physically from condensation of VOCs within a plume. The model also allows different optical properties for fresh and aged modes, where in the standard setup the aged mode is less absorbing due to the decreased proportion of BC contributing to the total mass (see Section 2.3). Since the 6 hr e-folding timescale is relatively short on a climate simulation timescale, most BBA in our simulations resides in the aged mode. Aged BBA exerts an indirect effect on clouds, and is converted to smoke-in-cloud-water by nucleation scavenging (analogous to sulfate aerosol in the model). BBA is removed by wet and dry deposition. In the simulations here, we adjust the optical and hygroscopic growth properties based on observations (see Section 2.3) as we find BBA in the CLASSIC scheme demonstrates too much hygroscopic growth and not enough absorption (see Johnson et al. (2016) for more details).

2.2 BBA Emission Experiments

This paper compares the results of two 30 year climate simulations with high and low BBA emissions. Fresh BBA emissions are injected into the atmosphere as surface emissions (in the lowest model level), as well as at high levels (model level 3 to 20 - roughly equivalent to altitudes up to 3 km) in order to represent burning plumes (which are not explicitly represented by the model) reaching higher altitudes.



Emission datasets are taken from Global Fire Emission Dataset (GFED) version 3.1 (van der Werf et al., 2010) for BC and OC. The emissions are summed to provide total BBA emissions in terms of carbon mass, allowing CLASSIC to incorporate oxygen mass and therefore calculate BBA mass. Emissions from GFED3.1 are provided in terms of vegetation sector: forest and deforestation fires provide high level emissions, while savannah, woodland and peat provide surface emissions. In all experiments the BBA emissions are scaled up by a factor of 2, in order to produce agreement between modelled and observed AODs, a measure that has been necessary in previous modeling studies using GFED3.1 (Reddington et al., 2015; Johnson et al., 2016, and references therein).

In order to test the sensitivity of climate to the BBA loading within the South American region (60S to 15N and -85 to -30W) we define two experiments to correspond to high and low emission cases, based on realistic variations of emissions observed for the South American region. During 1997 to 2011, the time period covered by GFED3.1 data, the highest emission year for the South American region was 2010, while the lowest emission year was 2000. Therefore high and low BBA emission experiments are defined using South American BBA emissions from 2010 and 2000 respectively. Total annual emissions for the high and low emissions experiments for the South American regions are 0.51 and 2.32 Tg respectively (including both high level and surface emissions). The geographical distribution of emissions for September 2000 and September 2010, the month of largest emissions, are shown in Fig 2. Outside of South America, BBA emissions are set to the 1997-2011 GFED3.1 mean, with monthly variations, and do not vary between experiments, in order to place the focus of the experiment solely on the impact of changing S. American emissions.

2.3 Hygroscopic Growth and Optical Properties in the Modified CLASSIC Scheme

This section describes how the hygroscopic growth and optical properties for BBA are altered from the standard CLASSIC values in order to be more in line with observations, including those from the recent SAMBBA intensive aircraft observations made during September 2012 (Johnson et al., 2016; Darbyshire et al., 2017, in prep.).

Fig. 3 shows the hygroscopic scattering growth curve ($f(\text{RH})$) of BBA in CLASSIC, and Fig. 4 shows the dependence of scattering, absorption, extinction and SSA on relative humidity. Optical properties in CLASSIC are derived from aircraft measurements made during SAFARI-2000 of southern African BBA (Abel et al., 2003) and scattering hygroscopic growth is taken from Magi and Hobbs (2003) (MH03), also for southern African BBA. CLASSIC allows for the separate representation of optical properties and hygroscopic growth of the fresh and aged BBA modes. $f(\text{RH})$ values at 80% RH are 1.5 and 2.2 for fresh and aged BBA respectively (see Fig. 4), demonstrating a very strong scattering increase at high humidities. Absorption in the model is not sensitive to RH (Fig. 4(b)), which is borne out by more recent measurements (e.g. Brem et al. (2012)). Since extinction is the sum of scattering and absorption, extinction in CLASSIC is also strongly sensitive to RH, as is the single scattering albedo (SSA) (Figs. 4(c) and (d)).

However, CLASSIC is not consistent with other measurements. For example, Kotchenruther and Hobbs (1998) performed aircraft measurements in the Amazon region around Brazilia, Cuiaba, Porto Velho and Maraba, and found much lower $f(\text{RH})$ values for BBA of 1.05 to 1.29 at 80% RH. Johnson et al. (2016) find that CLASSIC overestimates BBA hygroscopic growth, and therefore aerosol scattering, AOD and SSA in moist conditions. Therefore in this work, we apply the $f(\text{RH})$ curve of

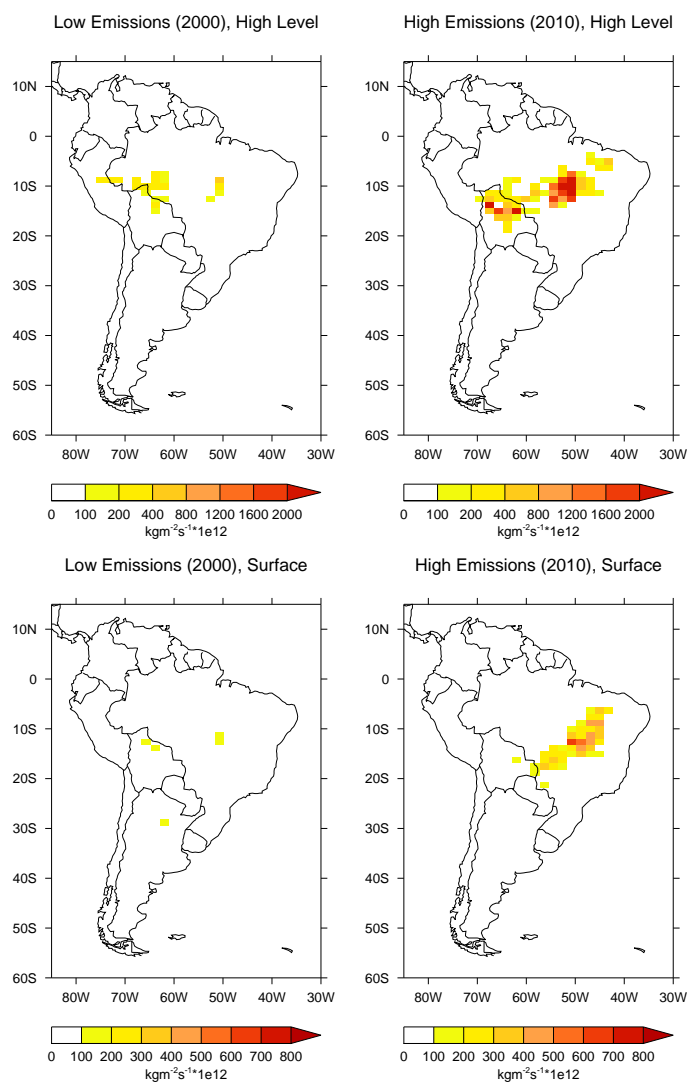


Figure 2. BBA September fire Emissions for the low (left hand side, 2000) and high (right hand side, 2010) emission experiments as applied in CLASSIC, from the GFED3.1 dataset. Upper panels show high level BBA emissions, lower panels show surface emissions. Note the different scales between upper & lower panels.

Kotchenruther and Hobbs (1998) from Porto Velho as a weakly hygroscopic case that gives a more reasonable representation, (as indicated by the green dashed line in Fig. 3) than the existing CLASSIC properties.

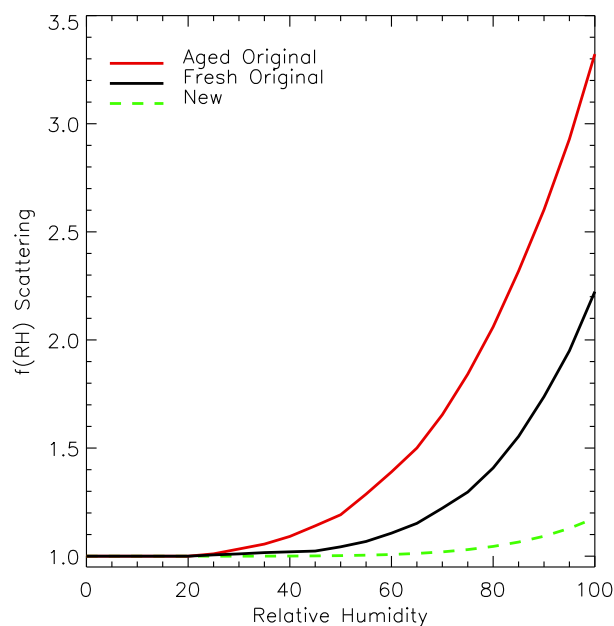


Figure 3. $f(\text{RH})$ scattering curves used in the CLASSIC aerosol scheme for BBA. Red and black show the standard hygroscopic scattering behaviour for fresh and aged BBA, green dashed line shows values applied in this work, taken from Kotchenruther and Hobbs (1998) for Porto Velho, Brazil.

Fig. 4 shows the new optical properties applied in this work. Scattering values are defined to be identical to the original CLASSIC aged values at 0% RH, but increase as a function of RH according to Kotchenruther and Hobbs (1998) for the more realistic Porto Velho BBA observations. The RH dependence and absolute values of absorption are kept identical to the original CLASSIC data. Since extinction is the sum of absorption and scattering, extinction at 0% RH is identical to the original CLASSIC data, but is much lower at high levels of moisture due to the lower $f(\text{RH})$ scattering dependency.

Additionally, although Fig. 4 shows a clear difference in optical properties in original CLASSIC between the fresh and aged BBA modes, the recent aircraft observations from SAMBBA did not reveal any differences between fresh and aged BBA, except possibly for very fresh BBA close to the source, under one hour from emission (pers. comm. W. Morgan). Therefore in these experiments, since fresh BBA represents aerosol within 6h of emission, we set the optical properties of fresh and aged BBA to be identical based on the new curves in Fig. 4.

As a result, the new SSA (Fig. 4(d), green dashed line) is close to the standard CLASSIC SSA values for aged BBA at low RH, and close to the standard CLASSIC SSA values for fresh BBA at high RH. The new values are also in agreement with long term inversion data from the AERosol Robotic NETwork (AERONET) stations (purple box) in the BB region, for 6 sites (L1.5 data from Ji Prana SE, Rio Branco, Alta Floresta, Abracos Hill, Balbina, Manaus EMBRAPA) which have more than

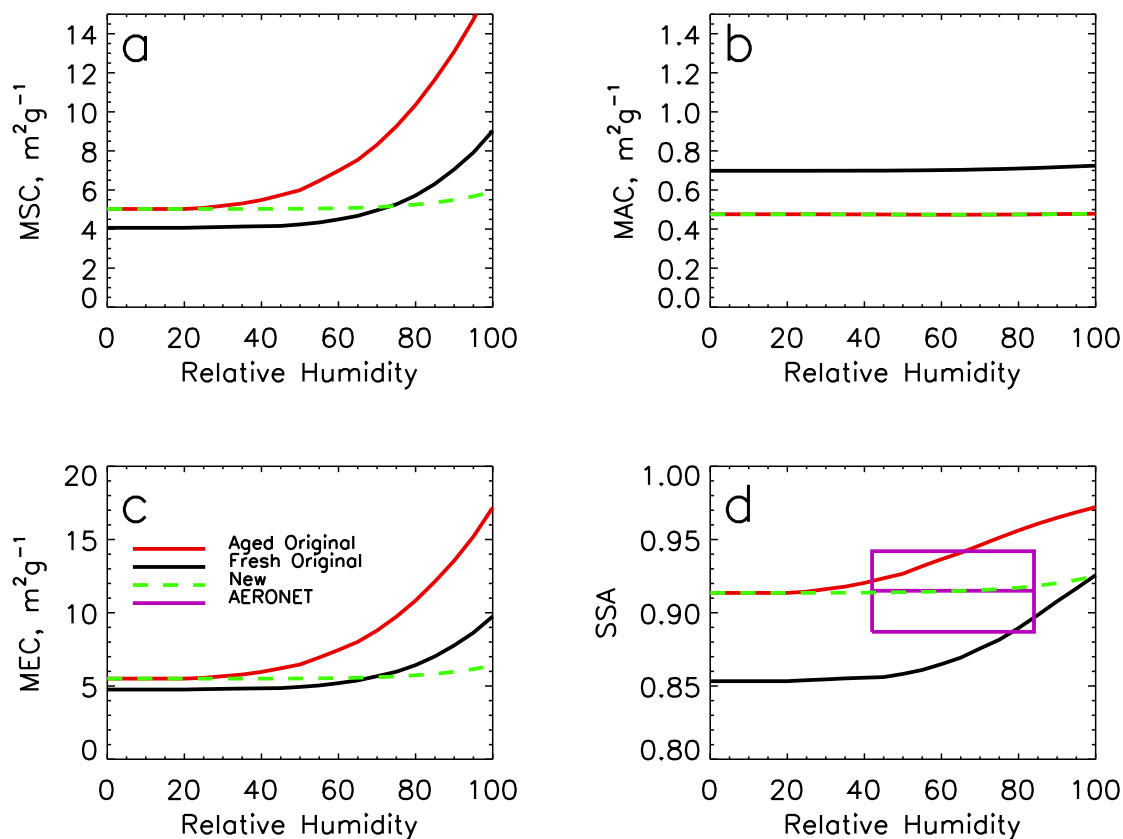


Figure 4. Optical properties used in the standard CLASSIC configuration for BBA at visible wavelengths (black: fresh BBA; red: aged BBA) and the new representations applied in this work for fresh and aged BBA (green dashed line). (a) Mass Scattering Coefficient; (b) Mass Absorption coefficient; (c) mass extinction coefficient; (d) single scattering albedo. AERONET SSA at 550nm is also shown (purple) with horizontal lines indicating long term maximum, mean and minimum (see text for details).

one year of data in the BB season (Aug-Oct). Horizontal lines shown in Fig. 4 represent maximum, mean and minimum SSA at 550nm (linearly interpolated between 440 nm and 675 nm) across the 6 sites. The range of RH covered by the AERONET box represents typical values encountered during the SAMBBA aircraft research flights.

A wide range of SSA values for BBA is indicated from different observations, as discussed by Johnson et al. (2016). For example, SAMBBA aircraft observations show that cerrado burning in the eastern regions produces more BC and less organic aerosol, and therefore a more absorbing BBA at 550 nm ($\text{SSA} = 0.79$), while forest burning in the west produces less absorbing BBA ($\text{SSA} = 0.88 \pm 0.05$) (Johnson et al., 2016; Hodgson et al., 2017). The range of AERONET retrievals shown in Fig 4 is 0.89 - 0.94 (mean 0.92). Satellite-based retrievals of BBA indicate even higher SSA values (pers comm. W. Morgan). Therefore



since the various observations of SSA vary greatly, an intermediate value of SSA of 0.92 at 60% RH seems reasonable for these experiments, as shown by the dashed line in Fig. 4(d). Further experiments were run with varied absorption but are not presented here. Optical properties in all of the six spectral bands covering the visible wavelengths were adjusted using the same procedure.

5 3 Impact of Biomass Burning Emissions in September

3.1 Introduction

September has the highest biomass burning (BB) emissions which can directly influence surface fluxes whilst in situ, so we look first at September monthly mean fields. For quantitative results we define a 'biomass burning box (BB box)' (from 5-15° S, 40-70° W), selected on the basis that this is the main area where AOD is affected by biomass burning aerosol. The statistical significance is determined by a t-test. We will examine the effects of the aerosol emissions on the AOD (aerosol optical depth), and the consequences of the AOD changes on the clouds, the longwave (LW) and shortwave (SW) radiation and the surface fluxes, and the surface temperature, pressure, circulation and precipitation. The results are shown in Table 1, which gives the mean effect within the BB box on several variables for the high emissions case, low emissions case, and the difference; (see figures for extent of the BB box).

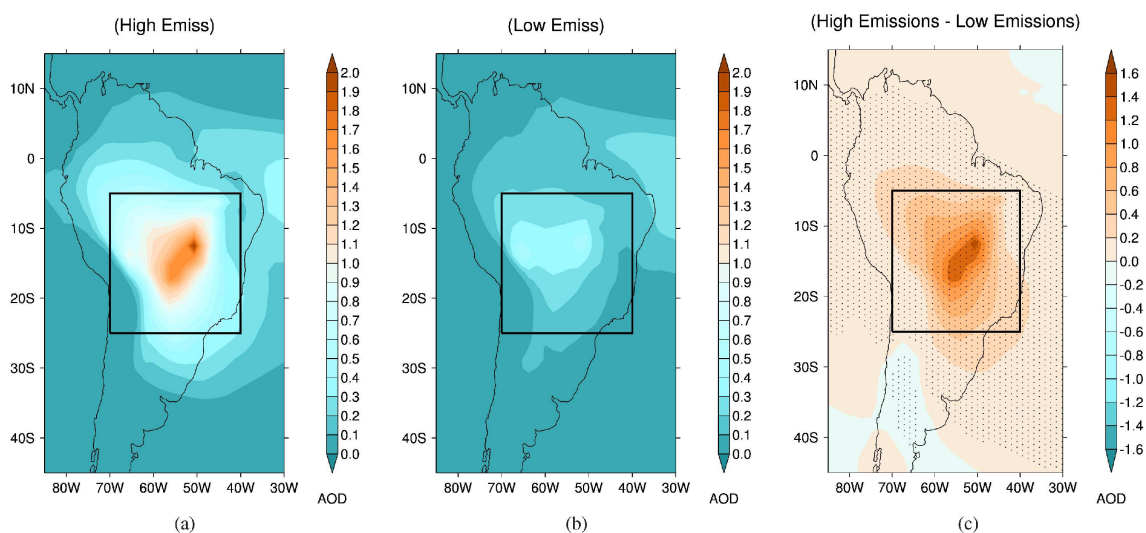


Figure 5. (a) The September mean biomass burning AOD at 0.44 μm for the high emissions experiment. The outlined box contains the area used to calculate mean values. (b) The September mean biomass burning AOD at 0.44 μm for the low emissions experiment. (c) Plot of the difference in the September AOD between the high and low emissions experiment, (H-L). Stippling represents 95% confidence limit.



Field	High	Low	Difference	% change [(H-L)/H]
AOD	0.68	0.19	0.48	70.6
Cloud Fraction	0.53	0.55	-0.02	-3.8
SW Down Surface (Clear Sky) (W/m ²)	284.56	298.34	-13.79	-4.8
SW Down Surface (All Sky) (W/m ²)	241.70	249.19	-7.42	-3.3
SW Net Surface (Clear Sky) (W/m ²)	237.35	248.85	-11.50	-4.8
SW Net Surface (All Sky) (W/m ²)	201.56	207.07	-5.51	-2.7
SW Up TOA (Clear Sky) (W/m ²)	75.31	71.98	3.33	4.4
SW Up TOA (All Sky) (W/m ²)	110.56	111.90	-1.32	-1.2
SW Net TOA (Clear Sky) (W/m ²)	328.01	331.34	-3.33	-1.0
SW Net TOA (All Sky) (W/m ²)	292.74	291.42	1.32	0.5
LW Up TOA (Clear Sky) (W/m ²)	287.26	286.73	0.53	0.2
LW Up TOA (All Sky) (W/m ²)	264.48	261.38	3.10	1.1
LW Net TOA (Clear Sky) (W/m ²)	-287.26	-286.73	-0.526	0.2
LW Net TOA (All Sky) (W/m ²)	-264.48	-261.38	-3.10	1.2
SW+LW Net Surface (Clear Sky) (W/m ²)	140.55	150.54	-9.99	-7.1
SW+LW Net Surface (All Sky) (W/m ²)	119.28	124.40	-5.12	-4.3
SW+LW Net TOA (Clear Sky) (W/m ²)	40.75	44.61	-3.86	-9.5
SW+LW Net TOA (All Sky) (W/m ²)	28.25	30.04	-1.79	-6.3
Sensible Heat Flux (W/m ²)	58.56	62.99	-4.32	-7.4
Latent Heat Flux (W/m ²)	59.12	60.90	-1.78	-3.0
Surface Temp (°C)	297.73	297.88	-0.14	0.0
Precipitation (mm/day)	1.78	2.05	-0.27	-15.2
Surface Pressure (mb)	945.38	945.60	-0.14	0.0

Table 1. Table of September mean values for the high and low experiments and the differences between them. The means are calculated over the biomass burning box (lat. 5-25° S, lon. 40-70° W), which is outlined in each figure.

3.2 AOD and Clouds

Fig. 5(a) and (b) shows the biomass burning AOD (BB AOD) at 0.44 μm over the 30 year HadGEM3-GA3 run for the high and low emissions case respectively. The high emissions case has a maximum BB AOD of approximately 1.6 across the central biomass burning area, and values of up to 0.3 extend to the north and south. The mean value for the outlined box is 0.68. In the low emissions case the highest values are 0.6, with lower values of 0.1 over most of the biomass burning area; the mean in the box is 0.19 (see Table 1). In both cases African biomass burning results in a small transported BB AOD across the S. Atlantic, which extends to the coast of S. America. In the two model runs, the biomass emissions from Africa (and the rest of



the world) are identical and are based on climatological means. The differences (high-low) in BB AOD between the two runs Fig. 5(c) are greatest over the BB region as expected; the BB AOD transported from Africa shows no difference between the two runs, confirming that this is not the result of S. American BBA. The mean BB AOD difference in the BB box area is 0.48, a reduction of 72% from the high case to the low case. As discussed in the previous section, the difference in emissions is 5 78% suggesting that the majority of the emissions change is translated to a BB AOD change. The direct relationship between particulate emission from fire and observed AOD in South America is noted by (Reddington et al., 2015).

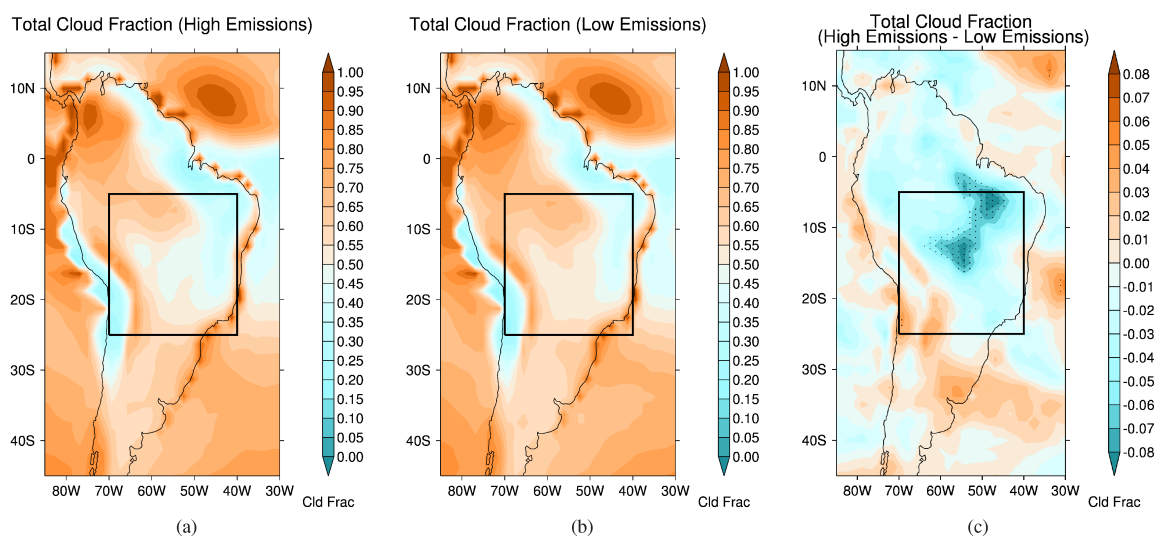


Figure 6. (a) The September mean cloud fraction for the high emissions experiment.(b) The September mean cloud fraction for the low emissions experiment.(c) Plot of the September difference in the cloud fraction between the high and low emissions experiment, (H-L). Stippling represents 95% confidence limit.

In Fig. 6(a) and (b) the total September average cloud fraction for the high and low emissions experiments are plotted, showing the distribution of cloud cover. In both cases the highest cloud fractions are over the far N.W. part of the continent, down into the Amazon basin. Along the east coast and into the Brazilian Highlands (centered on 15° S, 45° W) there is less cloud cover, although it increases again towards the Plate estuary (35° S, 58° W). There is also little cloud over the Andes, but a substantial fraction over the eastern edge of the Andes mountain range, and high cloud over the Caribbean area (12° N, 47° W). In Fig. 6 (c) the change in cloud fraction between the high and low emissions case is plotted - the stippled areas denote a confidence level of 95%. The cloud fraction is reduced by 0.05 in much of the biomass burning area (3.8% averaged over the BB box), although there is a substantial effect to the north-east of the main AOD difference (Fig. 5). The reduction in 10 cloud would be consistent with semi-direct effects found in other modelling studies, whereby increased atmospheric heating can reduce convective activity and burn-off the clouds within the aerosol layer (Koch and Del Genio, 2010). Outside of the area with high AOD differences higher emissions appear to result in a slight increase in cloud fraction in the area to the east 15

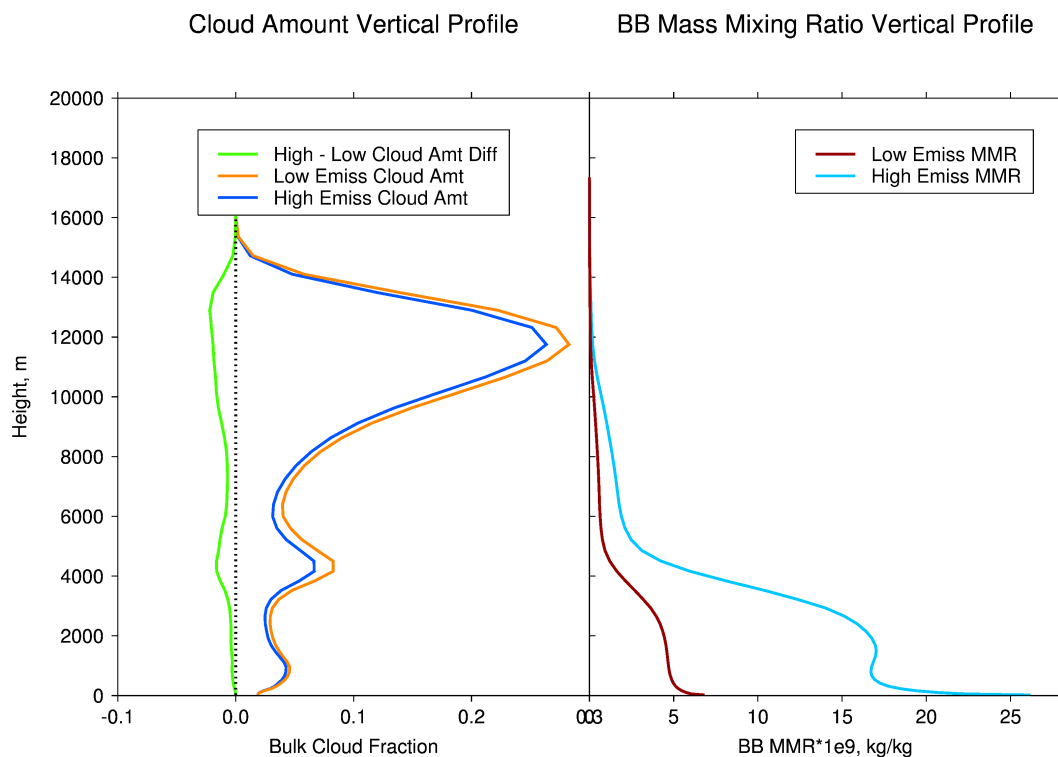


Figure 7. September mean vertical profile of cloud fraction for high emissions, low emissions, H-L compared with the vertical profile of the aerosol burden (mass mixing ratio in Kg/Kg) (both quantities averaged over BB box area outlined in area plots).

of the Andes and just north of the River Plate valley (34° S, 55° W); however the changes in these areas are not statistically significant at the 95% confidence level.

The profile of cloud fraction with height, averaged over the area outlined, is shown in Fig. 7 for the high and low emissions cases. The biomass burning burden profiles are shown for comparison. Cloud layers are evident at about 1 km, 4.2 km, and the presumed outflow from deep convective clouds at 9-14 km. Despite September being the dry season these clouds were frequently observed from the aircraft during the SAMBBA aircraft campaign (Marengo et al., 2016).

In general the low emissions case has more cloud at all levels, with the most marked differences in the high cloud amount at 9-14 km, and the mid-level cloud at 3-6 km. Cloud changes below 2 km are small, in part because cloud cover at these heights is minimal. Koren et al. (2004) suggest a reduction in boundary-level clouds can occur where aerosols stabilise the boundary layer and cool the surface, since the supply of water from the forest canopy is reduced. Where the aerosol and cloud are at the same height, i.e. below around 4 km, we would expect the reduction via the semi-direct effect to be strongest as the heating of the atmosphere due to the presence of absorbing aerosol promotes cloud evaporation (Koch and Del Genio, 2010). However



we see a similar magnitude of cloud reduction for the medium level (3-5 km) and the high clouds at 9-14 km, where the aerosol burden is much lower. A likely mechanism for this reduction in medium and high cloud cover would be the stabilising of the atmosphere, due to the aerosols in the lower levels heating the atmosphere but cooling the ground, stabilising the boundary layer, reducing its height, and thus reducing the amount of deep convection occurring in the high emissions case (Koren et al., 2008). In Fig. 8(a) the stable boundary layer diagnostic (which is defined to be set to 1 where the surface buoyancy flux is < 0.0, at each time step and each grid point; the average indicates the fraction of time in this state) shows that the high emissions case has a more stable boundary layer, especially in the areas where we see the most cloud reduction. This tends to support the explanation that cloud reduction is related to the boundary layer changes. The boundary layer height varies between 1 km and 1.8 km in the BB box, and in Fig. 8(b) the boundary layer height differences show a reduction for the higher BBA case, due to the reduction in SW radiation reaching the surface, and the reduction in sensible heat flux (Zou et al., 2017; Ackerman et al., 2000). The deep convection model diagnostic (defined to be set to 1.0 if deep convection occurs during a model a timestep, 0 if not, similar to the BL stability diagnostic mentioned above), shown in Fig. 8(c), also shows the statistically significant reduction in deep convection for the higher emissions case, across most of the main area of BBA, and also the area to the west side of the Amazon Basin. There is a dipole change in the Caribbean, where the area along the N.E. coast of S. America shows a statistically significant reduction, and just to the north there is a (statistically significant) increase for the high emissions case. Although this is not entirely congruent with the area of highest AOD difference, it is clear that there is a significant influence of BBA on the deep convection as represented by this diagnostic, suggesting that the reduction in cloud fraction may be due predominantly to this mechanism. This change in deep convection between simulations is likely to be contributing to the high and mid-level cloud changes, as in the model some of the mid-level cloud is likely due to detrainment of deep convective cloud around the freezing level.

Where evaporation is reduced and moisture availability for cloud formation are curtailed this would also act to inhibit cloud formation (Koren et al., 2008); the relative humidity (not shown) in the high emissions case is higher at the surface (< 1 km) by around 10 %, but lower throughout the rest of the profile, with the largest difference (-7.5 %) occurring at around 5 km. With a more stable boundary layer in the high emissions case there is less turbulent transport of moisture from the surface layer. This would suggest a drier atmosphere at height is also contributing to reduced cloud formation in the high emissions case.

Considering the indirect effect, in Fig.9 we see a reduction in the effective radius of the liquid water drops where increasing the aerosol amount reduces the effective radius, as suggested by e.g. Warner (1968); Twomey (1977); Jiang and Feingold (2006); Rosenfeld (2000). The vertically integrated droplet concentration also increases for the higher emissions case, which is consistent with predictions that the increase in nucleation centres (aerosol particles) will increase the number of droplets.

3.3 Effects on Radiation

In Fig. 10(a and b) we see the difference between the high and low emissions case in the downward SW at the surface, which largely follows the areal extent of the difference in the AOD. The results for the clear-sky (i.e. excluding all clouds) SW reaching the surface (in the BB box) from our models show the mean reduction in the September mean downwelling flux is -13.8 W/m^2 (a reduction of 4.8 %) for the high emissions case compared to the low emissions case. The All-sky differences

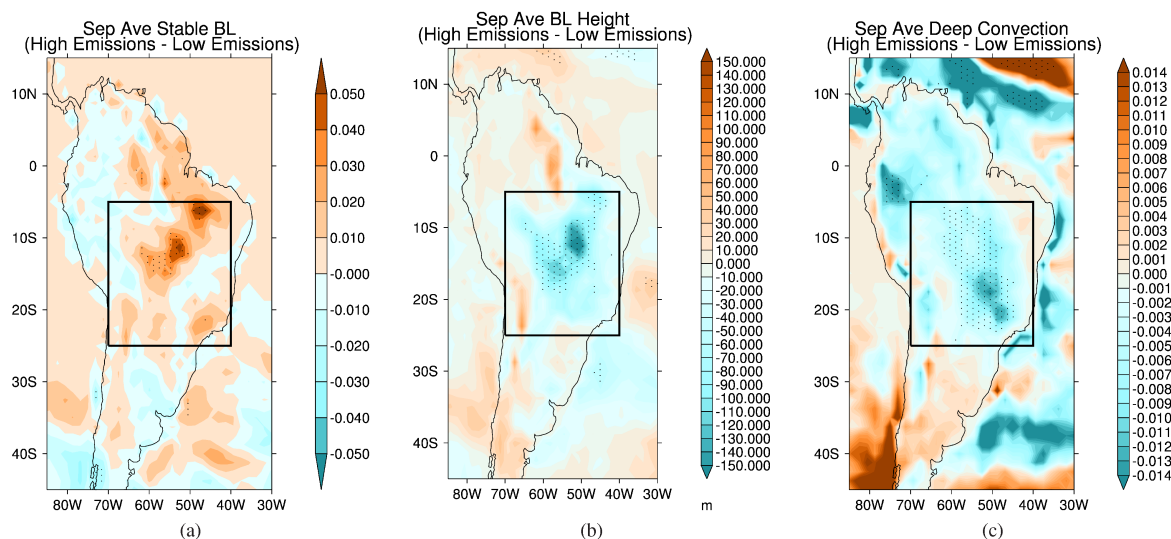


Figure 8. (a) Plot of the September difference in the boundary layer stability diagnostic between the high and low emissions experiment, (H-L). (b) Plot of the September difference in the boundary layer height between the high and low emissions experiment, (H-L). (c) Plot of the September difference in the Deep convection diagnostic between the high and low emissions experiment, (H-L). Stippling represents 95% confidence limit.

include the effect of clouds and indeed changes in the cloud fraction reduces the area mean change to -7.4 W/m^2 , indicating that scattering by the clouds above the aerosol reduces the difference we see due to the aerosol changes alone. The competing effects of the reduction in SW at the surface due to the BBA and the increase due to reducing cloud cover control the resulting impact on the SW at the surface, and in most of the BB box area the BBA has the stronger effect. There is also a statistically significant (at the 95% confidence level) surface reduction in SW to the north of the Plate Estuary (34° S , 55° W), which we interpret as the effect of the increase of cloud in this area, as the BB AOD difference is very small in this area, while the cloud fraction increases, (see Fig. 6(a)) resulting in the reduction of SW at the surface here.

The top of atmosphere (TOA) upwelling SW radiation differences are shown in Fig. 10(c and d), where the clear-sky differences show an increase for the high emissions case in the same area as the BB AOD differences between the two experiments. This illustrates the direct radiative effect, which is stronger with higher emissions. The all-sky case is much less clear cut, as the influence of the clouds results in a predominantly negative difference. This suggests that the effect of the reduced cloud cover, and thus reduced scattering by clouds in the high emissions case, dominates over the increased scattering from the increased BBA (as seen in the CS case). This changes the sign of the SW radiative effect at the TOA causing a net reduction in outgoing SW in the region. These changes are not statistically significant, however.

The difference in outgoing longwave (LW) radiation at the TOA is shown in Fig. 11, where the clear-sky difference shows a generally positive change, such that the increase in aerosol results in an overall increase in the outgoing LW radiation over

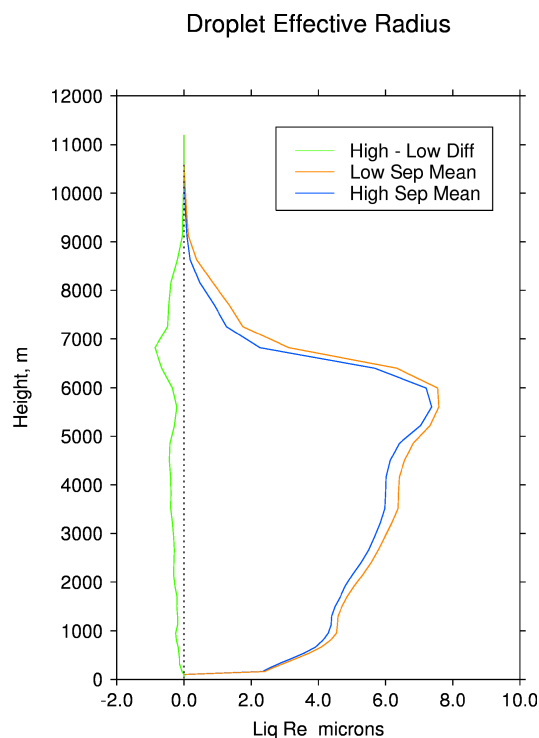


Figure 9. Vertical profile of September mean differences of droplet effective radius (microns) (averaged over the BB box 5-25° S, 40-70° W)

much of the biomass burning area. However, since the aerosol properties prescribed in the model relate to relatively small aerosol size the BBA has little effect on LW radiation directly. As the only significant changes are seen in areas outside the main biomass burning areas it is much more likely that these LW changes are related to secondary effects, for example water vapour changes. Shown in Fig. 11(c), the LW radiation changes are consistent with decreased column water vapour in the high emissions experiment, which leads to increased outgoing LW radiation at the TOA. The aerosol properties prescribed in the model relate to relatively small aerosol size therefore the effect of BBA on LW radiation is negligible. In the all-sky case, (Fig. 11(b)) the differences are significant in the main biomass burning area, but can be directly related to the changes in cloud fraction between the high and low emissions case; where the clouds are reduced, we see a greater LW upwelling at the TOA, as the effective emitting temperature is now lower in the atmosphere and warmer.

10 The clear-sky SW heating rate is shown in Fig. 12(a) for the high and low emissions results. The largest difference between the high and low emissions case is below 5 km, coincident with the majority of the absorbing aerosol, resulting in an increased heating rate of the atmosphere for the high emissions compared to the low emissions case. As the BBA is absorbing (with an SSA < 1.0) it absorbs some fraction of the SW and an increase in BBA results in an increase in the heating rate. The maximum heating rate also appears to be at a slightly lower altitude for the high emissions case. Above 5 km there is a much smaller

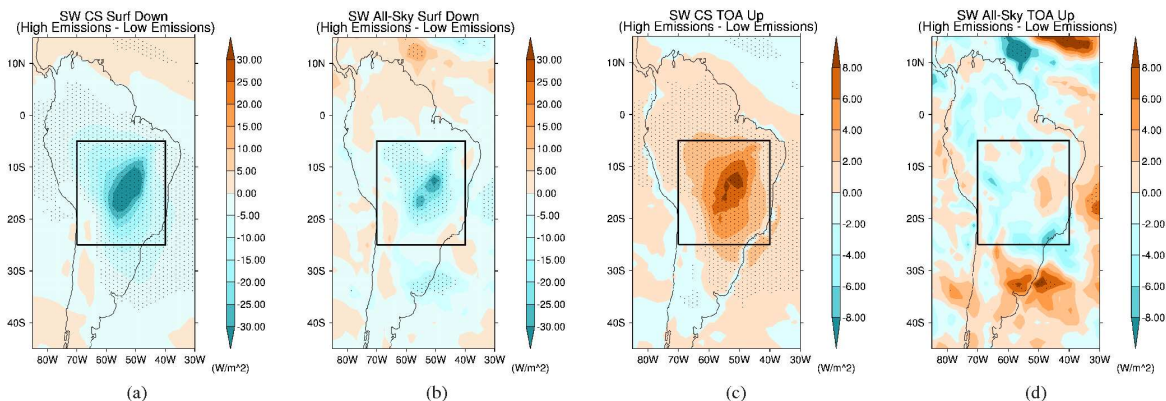


Figure 10. The September mean difference between high and low emissions case for (a) the clear sky downwelling SW radiation at the surface. (b) the all-sky downwelling SW radiation at the surface. (c) the clear-sky upwelling SW at TOA. (d) the all-sky upwelling SW at TOA.

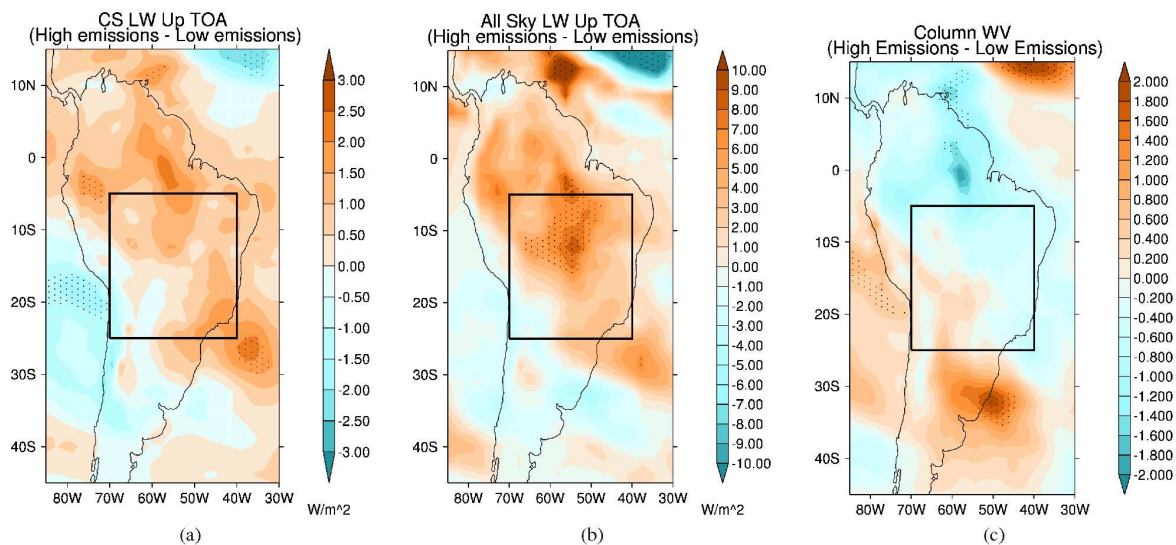


Figure 11. September mean differences (a) The difference between high and low emissions case for the clear sky outgoing LW radiation at TOA. (b) The difference between high and low emissions case for the all-sky outgoing LW radiation at TOA. (Note the colour scales for clear sky and all sky are different). (c) The difference between high and low emissions case for the column integrated water vapour.

difference, with a very slight negative difference at 9 km to 15 km (i.e. the high emissions have a slightly lower heating rate at this altitude).

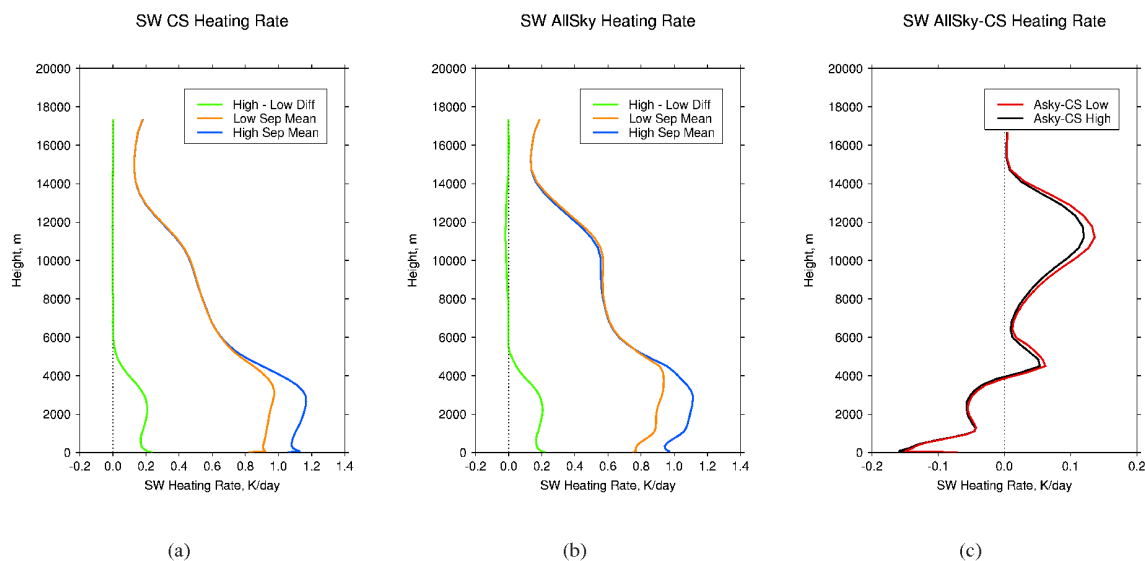


Figure 12. September mean SW heating rates (averaged over the BB box 5–25° S, 40–70° W) for high and low emissions (a) clear sky (b) all-sky (c) all sky - clear sky showing heating rate changes due to cloud only

The all-sky heating (Fig. 12(b)) rate shows broadly similar characteristics, but we see a dip in the heating rate in both cases at 500 m height, which is more marked in the high emissions case, and subsequently there is a less linear profile in both high and low emissions cases. The presence of clouds provides absorption and scattering of SW radiation above the main BBA layer resulting in an increase in the heating rate at levels containing clouds, relative to the clear sky case. The SW heating rate is reduced below the cloud, as less SW radiation reaches these altitudes and thus the heating rates here are reduced. The effect of the clouds is stronger in the low emissions case, as there is more cloud here, but the differences due to cloud cover compared to the clear sky are not large. The differences between the allsky-clear sky heating rates (Fig. 12(c)), illustrates the heating rate changes due to cloud only; beneath 4 km, clouds cause a cooling but differences between the two experiments are minimal. Above 4 km the clouds warm the atmosphere, with the extra cloud cover in the low emissions case producing a larger cloud heating rate than for the high emissions/reduced cloud case.

In Fig. 13(a) the clear sky LW heating rates show cooling up to 15 km (tropopause), with the largest cooling of -2.5 K/day at 4 - 5 km (note the difference in scales from the SW plots). The low emission experiments show less cooling than the high emission experiment below 6 km, which then reverses from 6-14 km. In the all-sky plot (Fig. 13(b)) we see below 4 km a reduction in cloud leads to more LW cooling of the lower atmosphere. Above 4 km, the reduced cloud leads to a slight warming of the atmosphere due to the upward longwave emissions from below. Higher BBA emissions reduce the cloud cover resulting in a reduction in the absorption of radiation, and thus less LW re-emission from the clouds. There may also be an increase in LW emission due to the increased temperatures in the BBA layer (0 - 4 km). The allsky-clear sky difference plot (Fig.13(c))

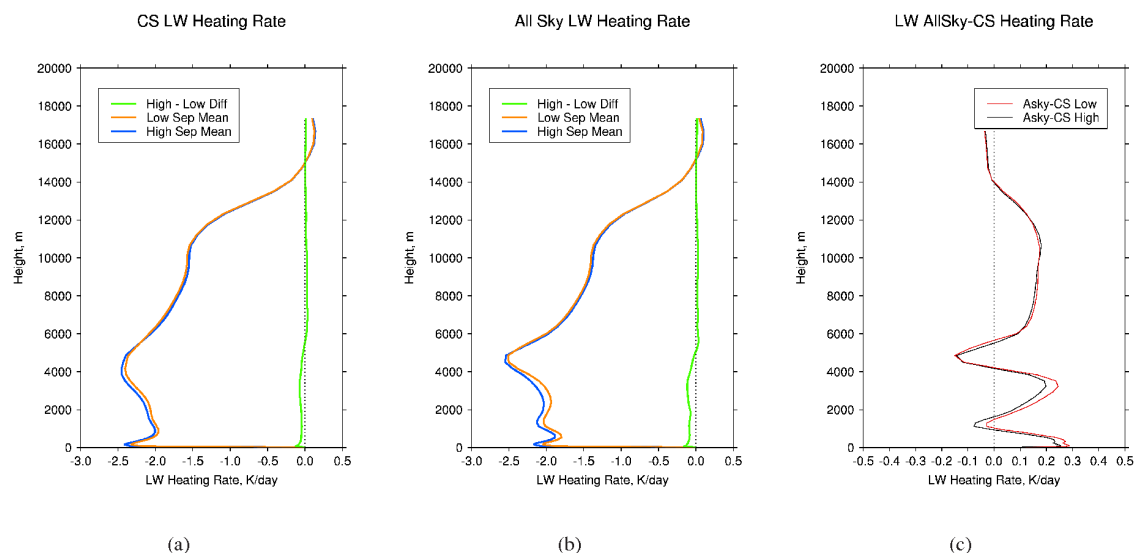


Figure 13. September mean LW heating rates (averaged over the BB box 5-25S, 40-70W) for high and low emissions for (a) clear sky (b) all sky (c) All sky - clear sky differences

shows the impact of the cloud changes alone on the heating rates, demonstrating the effect of higher emissions reducing the cloud cover, and reduced heating between the cloud layers (e.g. near the surface and at 3 km) and increased cooling within the cloud layers (1 km and 4 km), but there is very little change at higher altitudes. Within the BBA layer we can see the heating rates semi-direct effect of the cloud burn-off, but the higher cloud (12 km and above) appear to be responding to stability changes.

The effects of the BBA on the sensible heat flux are shown in Fig. 14(a), where the higher emissions result in a reduced sensible heat flux, due to the reduction in SW radiation cooling the surface (c.f. Fig. 10(b)). There are also significant differences around the R. Plate estuary, which may be due to an increase in cloud cover in this area for the high emissions case which reduces the SW radiation reaching the surface, and thus also reduces the sensible heat flux. The agreement spatially with the main differences in BB AOD (see Fig. 5) is generally good, suggesting this is largely an effect of the increased BB AOD in this case. The latent heat flux differences show statistically significant reductions for the high emissions case in the area to the north of, and in the centre of, the main BB area. However these changes are not strongly co-located with the BB AOD changes and are possibly related to reductions in available moisture due to reduced precipitation and circulation changes affecting the latent heat flux, which are investigated in the next section. These results are consistent with those of Zhang et al. (2008).

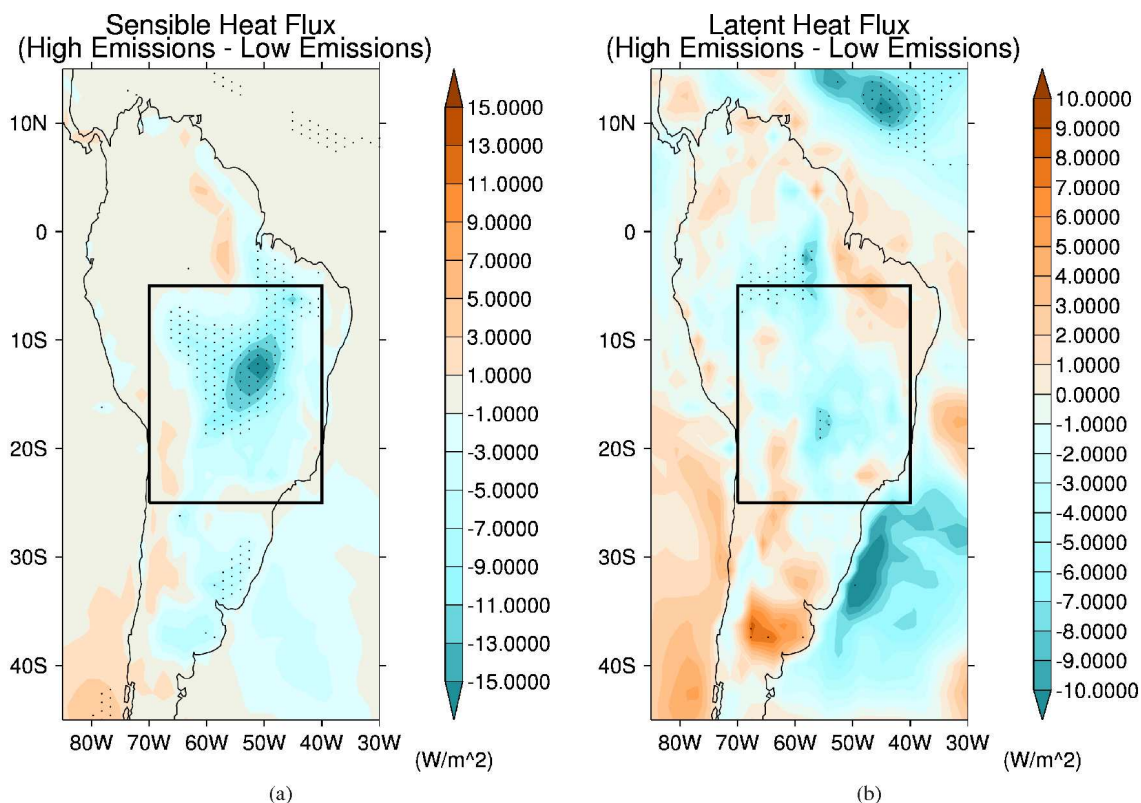


Figure 14. (a) September mean differences (high - low) for (a) sensible heat flux (b) latent heat flux. Stippling represents the 95% confidence interval.

3.4 Meteorology

There is a mean change (in the BB box) in the surface temperature between the high and low emissions runs of $0.14\text{ }^{\circ}\text{C}$, with the largest decrease of approximately $0.8\text{ }^{\circ}\text{C}$ in the north part of the BB box, and a maximum increase of approximately $0.5\text{ }^{\circ}\text{C}$ around the southern part of the Brazilian highlands (25° S , 50° W) as shown in Fig.15(a)). The spatial pattern here reflects the BB AOD differences in part, where the absorption and scattering of SW by the aerosol reduces the surface temperature. There are increases in surface temperature where the clouds are reduced near the southern Brazilian Highlands; here the cloud reduction allows more of the SW radiation through, and the extinction due to the BBA is somewhat lower than in the north of the box. The competing effects of the direct effect reducing the SW radiation reaching the surface and the reduction in cloud cover increasing the SW radiation at the surface are clear, controlling the mixed geographical response of the surface temperature overall.

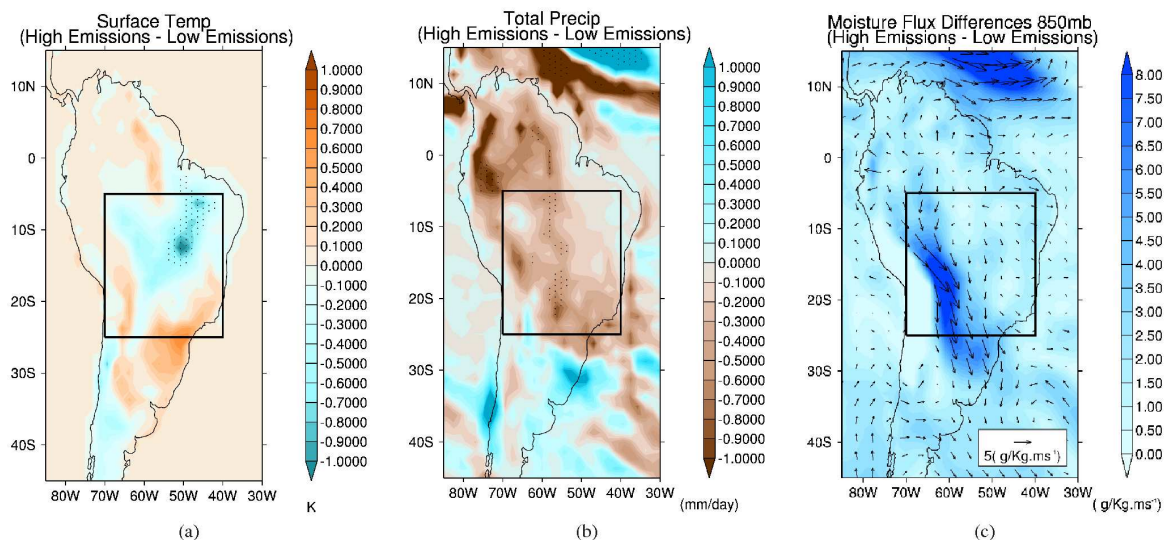


Figure 15. September mean differences (high - low) for (a) surface temperature (b) total precipitation (Stippling represents the 95% confidence interval) (c) moisture flux differences at 850 mb, coloured contours are the magnitude of the moisture flux.

The differences in total precipitation are shown in Fig. 15(b), where the overall effect in much of the northern part of the continent is a reduction in the total precipitation, particularly marked in the western Amazon basin and the Caribbean. Further south we see an increase in the area just north of the River Plate (30° S, 55° W), which corresponds to the area of increase in cloud fraction seen in Fig. 6. The decreased aerosol in the low emissions case leads to a 14 % increase in precipitation in the BB box with mean precipitation increasing from 1.78 mm/day (high emissions) to 2.05 mm/day (low emissions).

The decrease in precipitation seen in the high emissions experiment is consistent with the reduced cloud and latent heat flux, and the more stable boundary layer seen in this experiment. The resulting reduction in precipitation could result in a reduction in soil moisture content, partly explaining the reduction in latent heat flux shown in Fig. 14(b). Gonçalves et al. (2015) analysed rainfall data in the Amazon and suggest that the influence of biomass burning on precipitation is dependent in part on the degree of atmospheric instability. In a more stable atmosphere, BBA tends to decrease the precipitation; they also note that increasing cloud droplet number, and decreasing droplet size, would act to reduce precipitation in the absence of strong convection. In Fig. 15(c) the moisture flux at 850mb shows the increase of moisture transported by the low level jet east of the Andes, which together with the increased flux from the S. Atlantic combines to produce the increase in precipitation seen at 30° S, 50° W.

The surface pressure and 850 mb circulation for high and low emissions are shown in Fig. 16(a) and (b). The ERA-Interim mean September surface pressure and circulation (averaged over a similar time scale) are shown in the Supplemental material (Fig. ?? and Fig. ??) for comparison, and show that in general both surface pressure and the circulation are well represented by the model, although the wind flow seems to be somewhat more zonal between 0-10° S in the ERA-Interim plot. The model results for surface pressure are broadly similar for both the high and low emissions experiments, with a high pressure area in the

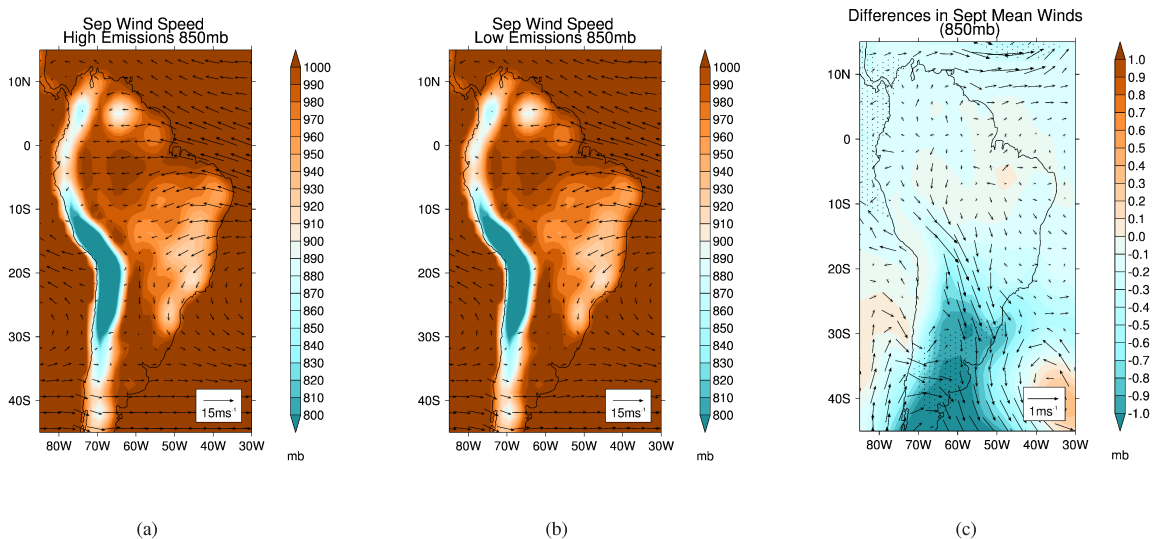


Figure 16. September mean wind circulation at 850 mb for (a) high emissions case. Coloured contours are mean September pressure in mb. (b) low emissions case. Coloured contours are pressure in mb. (c) differences in pressure and wind circulation for high - low runs. Coloured contours are pressure differences in mb.

central Amazon basin, and low pressure to the north and west. We also see high pressure along the eastern side of the Andes, down towards the River Plate estuary, and a high pressure system in the south east Atlantic, which shows some difference in position between the high and low emissions case. The surface pressure differences (Fig. 15(c)) show a slight increase in the Amazon basin area, but a larger decrease down in the southern part of Brazil and around the Plate Estuary. We also see a difference in the S. Atlantic, which is related to the position of the S. Atlantic high shifting between the high and low emissions case. The pressure differences are of the order of 1mb, with significant changes at the 95% confidence level in the Caribbean area and in S. Argentina.

The change in pressure patterns corresponds to the change in winds at 850 mb (Fig. 16(a) and (b)). The general circulation is easterly across the Amazon basin, south-easterly in the Caribbean, and tending to north-easterly to the south of the Amazon mouth. In the southern part of Brazil we see a northerly direction, turning westerly at the southern tip of the continent. Although the overall circulation patterns are similar for the two experiments, we do see differences between the high and low emissions case in Fig. 16(c), the largest effect being a strengthening of the low level jet that runs along the eastern side of the Andes, from around 10° S to 30° S, down to the Plate Estuary. Analysing the zonal and meridional components suggests that the most significant change is in the zonal component possibly suggesting a change in direction as well as in strength. There is also a change in the circulation due to the shift in the S. Atlantic high pressure system, where the easterlies are weaker in the low emissions case, and have a more southward component in the high emissions case. In the Caribbean area the prevailing easterlies and south-easterlies are weaker in the high emissions case.



4 Impacts on the Monsoon

We investigated whether or not there was a significant impact of the BBA on the South American monsoon by comparing precipitation and circulation differences between the high and low emissions cases for the monsoon onset months of September, October and November. As we do not have model results output on a daily basis, we cannot resolve the question of whether the detailed timing of onset of the monsoon is affected by the BBA using these experiments. However, we can examine whether the effects of the August-September peak biomass burning carry through the monsoon onset in October to November, using the monthly means to compare the meteorology between the high and low emissions case.

4.1 Evolution from September to November

The changes in the wind circulation from September to November can be seen in Fig. 17, with the winds at 850 mb for the two emissions cases and the differences between them shown for the three months. The overall evolution of the circulation from September to November broadly follows the predicted patterns (Raia and Cavalcanti, 2008; Marengo et al., 2001, 2012) for monsoon development in both high and low emissions cases. In October the overall circulation is similar to that for September, although there is a shift from easterlies to northerlies and north-easterlies across the Amazon basin; as we move into November this trend towards northerly and north-easterly winds becomes more pronounced, particularly in the western Amazon basin where by November the winds are northerlies. In the Atlantic close to the Amazon mouth we see a shift from the south-easterlies to more easterlies, a trend which continues into November. The (northerly) low-level jet along the eastern side of the Andes strengthens as we go from September to November, and the S. Atlantic high pressure system shifts westwards and decreases, with a corresponding shift in the circulation in the S. Atlantic and the S.W. coastal areas of the continent (Marengo et al., 2012). In November the changes show the clear shift from easterlies in the equatorial area in September to north-easterlies and northerlies, which exemplifies the change from zonal to cross-equatorial flow as discussed in Marengo et al. (2001). The N. Atlantic trade winds strengthen in the equatorial area in November, and the change in E. Brazil from easterlies in September to north-easterlies in November (Raia and Cavalcanti, 2008) is apparent, and is due to the displacement in the S. Atlantic high from September to November. The low level jet along the E. Andes becomes stronger, and in general northerlies run down the centre of the continent.

The changes in pressure from September to November (Fig. 18) show a general decrease (in both emissions cases) overall which is most marked along the eastern edge of the S. Andes, and down towards the Plate/Salado valleys (20° S, 65° W down to 40° S 65° W). The S. Atlantic high shifts eastwards, and reduces somewhat in strength from September to November (18(a-d-g), as described in Raia and Cavalcanti (2008). In September (Fig. 18(a-c)) the pressure shows the S. Atlantic high and a S. Pacific high, on each side of the continent at 30° S. We see low pressure related to the topography in the Andes, Guyana Highlands and the Brazilian highlands. In October, Fig. 18(d-f), the small high pressure system in the central Amazon shrinks slightly in size, and we see the S. Atlantic high shifting eastwards. The S. Pacific high appears to increase slightly in size, especially in the high emissions case. The surface pressure in November (Fig. 18(g-i)) shows the S. Atlantic high pressure

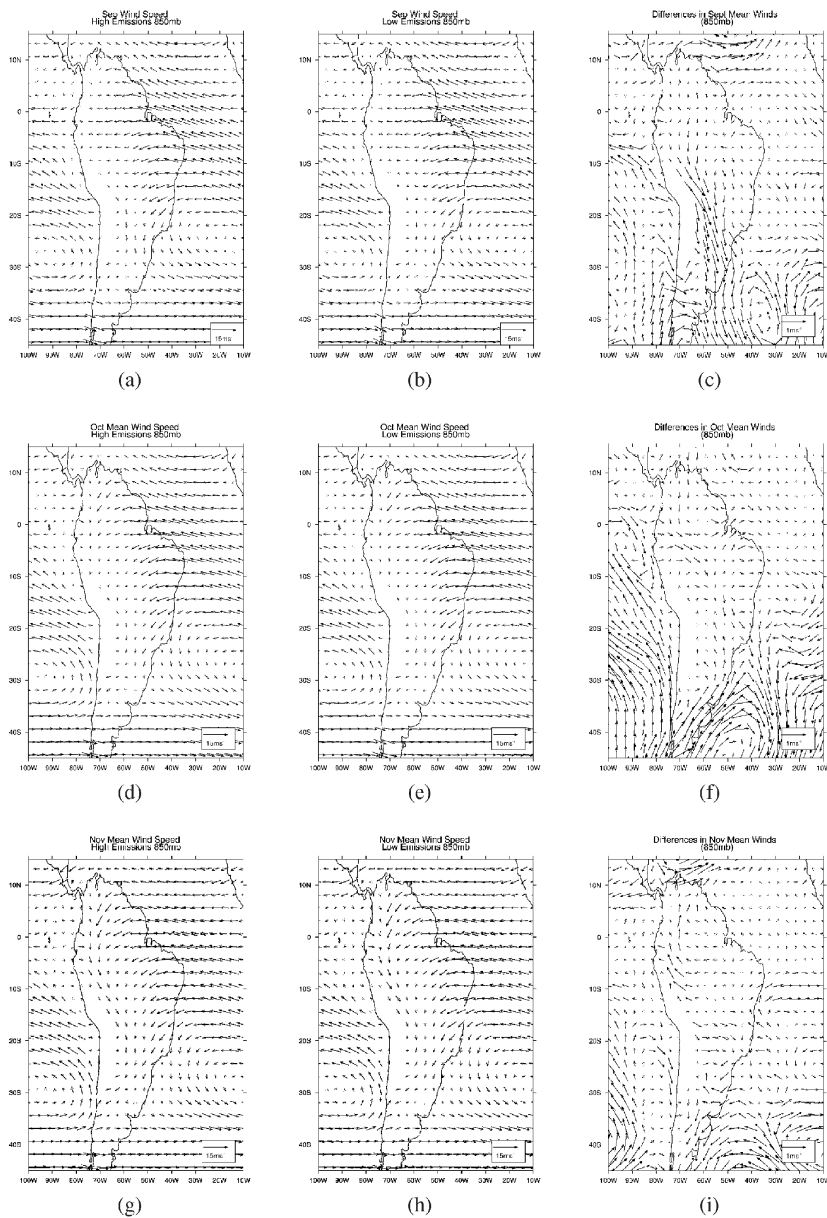


Figure 17. Mean monthly circulation (a) Sept High emissions. (b) Sept Low emissions. (c) Sept differences (H-L) (d) Oct High emissions. (e) Oct Low emissions. (f) Oct differences (H-L) (g) Nov High emissions. (h) Nov Low emissions. (i) Nov differences (H-L) Note the difference in projection and area from previous plots)



region shrinking in size and moving further eastwards, and the S. Pacific high also shrinking slightly, There is a decrease in pressure between the N.E. coast of S. America and W. Africa, which is more pronounced in the low emissions case.

The development of the precipitation from September to November clearly shows the extension of the high precipitation amounts in the western Amazon towards the south and west, indicative of the beginning of the wet season across the central part of S. America. The September precipitation shows high precipitation in the western Amazon basin and north of the equator, and lower values throughout the rest of the continent, especially dryer in the Atacama desert and over the Brazilian Highlands. The levels outside of the western Amazon are around 7 mm, down to < 0.5 in the dryer areas. Moving to October we see the higher precipitation spreading southwards down the west coast, and across towards to the east coast in the northern part of the continent. November precipitation as shown in Fig. 19(i) shows this area of increasing precipitation moving southwards and eastwards, although the area at the northern tip of the Brazilian Highlands and the N.W. coast remain at a similar level of precipitation as in October. The pattern of increasing precipitation from September to November we observe here is broadly in line with the predictions for the monsoon onset in this region (Raia and Cavalcanti, 2008; Liebmann and Mechoso, 2011).

4.2 Differences Between High and Low Emissions for September to November

We have already discussed the main circulation differences between the high vs. low emissions for the September case in 3.4; we noted that the low-level jet along the east side of the Andes is affected by the BBA, and the circulation in the S.E. Atlantic is altered (see Fig. 17(c)). The October differences between high and low emissions are shown in Fig. 17(f)), where we see little difference over the Amazon, with the largest changes along the west coast in October showing a greater northward component in the high emissions case in the westerlies, and the circulation evident at 20-30° S and 90° W also shows a strengthening of the northward component in the high emissions case. Around the S. Atlantic area there is again a more northward and north-eastward tendency along the coast for the high emissions, turning to a larger southern component out at 35° S, 30° W - these changes are most likely related to changes in the S. Atlantic high. The differences between the high and low cases in November are less striking although we still see the effects of changes in the S. Atlantic and there are also residual differences in the S. Pacific (Fig. 17(i)). As the position of the S. Atlantic high is affected by the aerosol emissions the changes in the circulation and thus the moisture flux in this area could be ascribed to the BBA. There is also a weakening of the easterlies at 0-10° N in the atlantic area for the high emissions case, and some increase in the low level jet on the east side of the Andes, but only south of 15° S, 70° W; north of this point the flow is weakened in the high emissions case.

The differences in surface pressure between high and low emissions for September (Fig. 18(c)) show a slightly higher pressure around the Amazon basin, and in the S. Pacific and S. Atlantic, although these latter two changes are most likely related to changes in the positions of the respective high pressure systems. There is a larger change in the southern end of the continent, from 25° S down to the southern tip, which is significant at the 95% confidence level. There is also a statistically significant pressure reduction along the N.W. coast and out across the equatorial pacific. The differences plot for October (Fig. 18(f)) reflects these changes, with the largest statistically significant changes in the S. Atlantic and S. Pacific. We also see statistically significant changes from the western Amazon basin down the E. side of the Andes to the southern edge of the Brazilian highlands. The other large area of statistically significant difference is across the Atlantic between W. Africa and

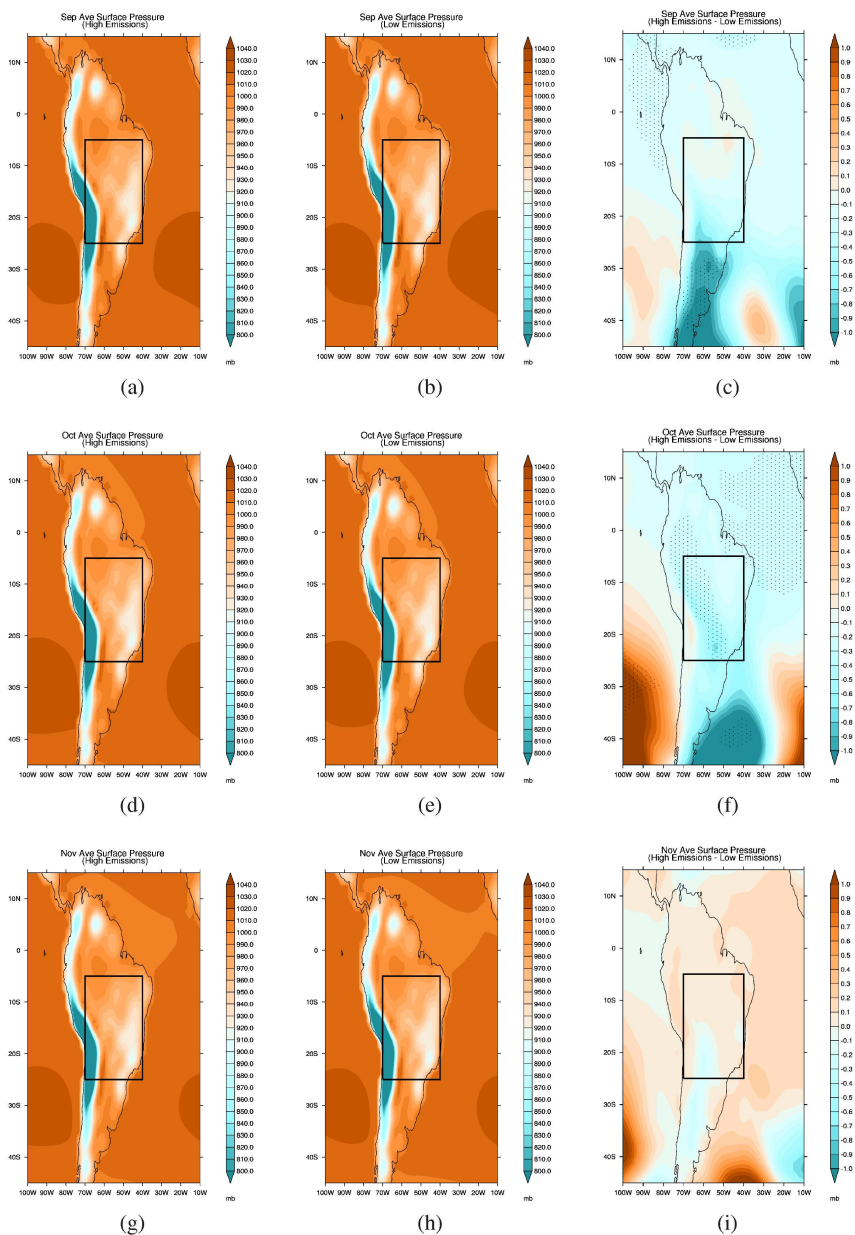


Figure 18. Mean monthly surface pressure (a) Sept High emissions. (b) Sept Low emissions. (c) Sept differences (H-L) (d) Oct High emissions. (e) Oct Low emissions. (f) Oct differences (H-L) (g) Nov High emissions. (h) Nov Low emissions. (i) Nov differences (H-L) Note the difference in projection and area from previous plots)



the N. Eastern edge of S. America. In November the difference plot (Fig. 18(i)) shows no statistical significance in the changes, but the S. Atlantic and S. Pacific changes are still evident. The changes in the rest of the continental area are small, with a switch to a positive difference (H-L emissions) in the areas of the Amazon Basin and the eastern parts of the BB box. It is clear there are statistically significant differences in surface pressure that extend into October, but the changes in November are generally smaller in magnitude and not significant.

The precipitation differences between the high and low emissions cases for September were discussed in Section 3.4, where we noted an overall reduction in precipitation in the BB box and Amazon basin, and an increase to the north of the Plate estuary (Fig. 19(c)). October precipitation differences (Fig. 19(f)) are mixed, with increases in the Amazon Basin, and in parts of the Brazilian Highlands, and decreases in the centre of the BB box and the Gran Chaco area (centred at 25° S, 60° W), down to the area between the Plate estuary and the southern edge of the Brazilian Highlands. However, the only areas with statistical significance are around the areas N. and W. of the Plate estuary. The mean differences in precipitation for November are shown in Fig. 19(i), where we see the area of reduced rainfall is quite extensive, extending from the Amazon basin down the east of the Andes to the Plate estuary (35° S 60° W). The areas in the NW corner of the BB box, and the E. side of the Andes towards the Plate Estuary all show significant differences at the 95% confidence level, and could be related to changes in the circulation, increased convective stability and the moisture fluxes in these areas (Collini et al., 2008). We also see significant differences in the S. Atlantic area, which could be related to changes in circulation as a result of the difference in the position of the S. Atlantic high pressure system between the high and low emissions case. Precipitation increases around the Brazilian Highlands, although this is not statistically significant at the 95% confidence level. The changes in the precipitation due to the BBA are significant in a few areas, suggesting that there is a continuation of the effect of the BBA on precipitation through to November, and thus on the monsoon. Overall, there is an effect on several parameters related to the monsoon development, which could be interpreted as affecting the monsoon development. However, within the constraints of the experiments performed so far, it is difficult to suggest how much, and what kind, of an effect there may on the monsoon as a result of the biomass burning.

5 Discussion and Conclusions

The aim of the work described here was to investigate the impact of biomass burning emissions on the regional climate in S. America using the Met Office Unified Model HadGEM3 GA3 model. We have found clear semi-direct effects of the biomass burning aerosol in September, with the results indicating a significant burning off and an additional effect on cloud cover from reduced deep convection, as the aerosols stabilise the boundary layer and suppress surface fluxes. Changes in the cloud microphysical properties (i.e. effective radius of the droplets) are evidence for the 1st indirect effect occurring as a result of increased BBA. The changes in the SW radiation for higher BB emissions are as expected from the direct effect, with a reduction in downwelling SW radiation at the surface and an increase in outgoing SW radiation at the TOA in the clear-sky case. The all-sky (cloud effects included) case shows less of a reduction at the surface, due to the decrease in cloud cover which indicates that the BBA dominates the surface radiation SW flux while simultaneously decreasing cloud cover. The effect on the outgoing SW radiation at the TOA is more mixed. The LW radiation changes are controlled mainly by cloud changes,

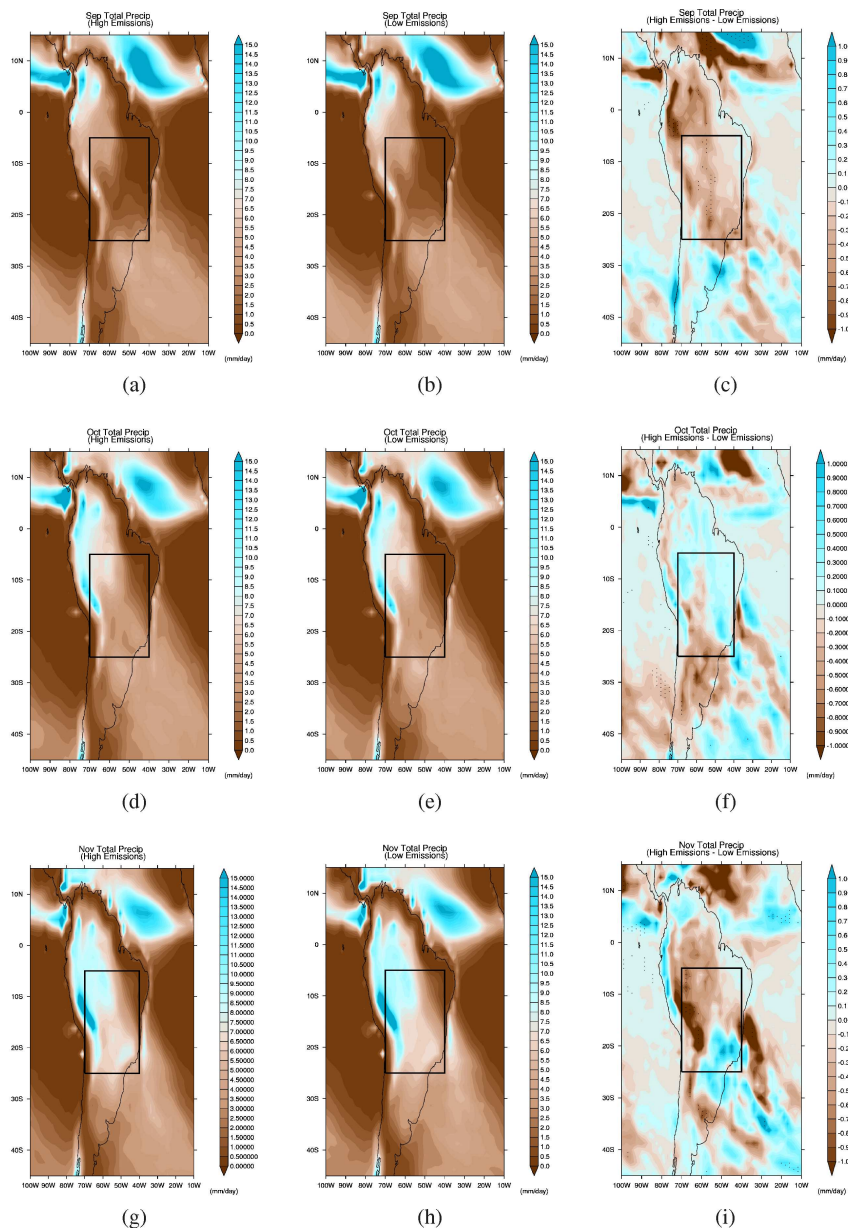


Figure 19. Mean monthly total precipitation - note that blue represent high values, brown low values. (a) Sept High emissions. (b) Sept Low emissions. (c) Sept differences (H-L) (d) Oct High emissions. (e) Oct Low emissions. (f) Oct differences (H-L) (g) Nov High emissions. (h) Nov Low emissions. (i) Nov differences (H-L) Note the difference in projection and area from previous plots



although WV changes induced by the BBA also contribute. Atmospheric heating is increased in the presence of more aerosol, and surface fluxes respond to the reduction in the surface SW radiation with both the sensible and latent heat fluxes being reduced. The reduced SW radiation also lowers the surface temperature, where a combination of the aerosol and the aerosol-cloud interactions causes reductions in surface temperature in areas of higher BB AOD, and an increase in areas where the cloud cover is sufficiently reduced to counterbalance the cooling effects of the BB AOD. There is a potential feedback from the reduction in SW radiation at the surface and heating by the aerosol at higher altitudes causing cloud burn-off and increased BL stability; the increased stability reduces cloud generation and leads to a further reduction in the cloud cover. This process will break down if the increase in SW radiation reaching the surface due to loss of cloud cover dominates over the BBA effects, allowing the BL to once again destabilise (Koren et al., 2008). The mean September precipitation in parts of the BB area is significantly reduced (up to 15 %) in the BB box, with some reduction also occurring in parts of the Amazon basin, most marked towards the western edge. There is also an effect on the surface pressure and changes to the low-level (850mb) circulation, in particular the low-level jet east of the Andes and the S. Atlantic high pressure system.

The impact on the monsoon is less clear cut, however we see distinct differences in November between the high and low emissions experiments. The changes in the surface pressure and circulation, in particular the low level jet which brings moisture down from the Amazon, and the shift in position of the S. Atlantic high pressure system affect monsoon development ((Raia and Cavalcanti, 2008). There is significant reduction in precipitation along the eastern side of the Andes and around the Plate Estuary area. These changes in the precipitation due to the BBA suggest that there is a continuation of the effect of the BBA on precipitation through to November, and thus on the monsoon. We note that in order to see any possible effects on the timing of monsoon onset a finer temporal resolution in the model output would be required. A further caveat is that the model is not a fully coupled atmosphere-ocean model, so the atmospheric changes do not influence the sea surface temperature (SST) so that effects of sea surface temperature changes, in particular on the monsoon development (Marengo et al., 2001; Liebmann and Marengo, 2001), are not being modelled in these experiments. The experiments described use emission inputs (from GFED version 3.1) for two different years in order to gauge how the climate effects differ between years with high and low emissions instead of comparing a BBA-free atmosphere with a high BB aerosol case. Our approach does tend to lessen the signal to noise in the results compared to a biomass burning vs. no biomass burning comparison, but allows us to demonstrate that significant climate differences can result from the realistic annual variations seen in the BB emissions in S. America.

Author contributions. C.L.R set up and performed the model runs for which B.T.J. provided emissions files. G.D.T analysed the model run results. G.D.T. prepared the manuscript, C.L.R. wrote the model set-up sections and all authors contributed to scientific discussions and helped in writing the manuscript.

Competing interests. The authors declare no competing financial interests.



Acknowledgements. This work was funded by the Natural Environment Research Council (NERC) through the South American Biomass Burning Analysis (SAMBBA) project under NERC grant number NE/J008435/1. This work used the ARCHER UK National Supercomputing Service to perform the model experiments. The Facility for Airborne Atmospheric Measurement (FAAM) BAe-146 Atmospheric Research Aircraft is jointly funded by the Met Office and Natural Environment Research Council and operated by DirectFlight Ltd. We would like to thank the dedicated efforts of FAAM, DirectFlight, INPE, the University of São Paulo, and the Brazilian Ministry of Science and Technology in making the SAMBBA measurement campaign possible.



References

- Abel, S. J., Haywood, J. M., Highwood, E. J., Li, J., and Buseck, P. R.: Evolution of biomass burning aerosol properties from an agricultural fire in southern Africa, *Geophysical Research Letters*, 30, doi:10.1029/2003gl017342, 2003.
- Ackerman, A. S., Toon, O. B., Taylor, J. P., Johnson, D. W., Hobbs, P. V., and Ferek, R. J.: Effects of Aerosols on Cloud Albedo: Evaluation of Twomey's Parameterization of Cloud Susceptibility Using Measurements of Ship Tracks, *Journal of the Atmospheric Sciences*, 57, 2684–2695, doi:10.1175/1520-0469(2000)057<2684:EOAOCA>2.0.CO;2, [https://doi.org/10.1175/1520-0469\(2000\)057<2684:EOAOCA>2.0.CO;2](https://doi.org/10.1175/1520-0469(2000)057<2684:EOAOCA>2.0.CO;2), 2000.
- Albrecht, B.: Aerosols, cloud microphysics, and fractional cloudiness, *Science*, 245, 1227–1230, cited By 1713, 1989.
- Allan, J. D., Morgan, W. T., Darbyshire, E., Flynn, M. J., Williams, P. I., Oram, D. E., Artaxo, P., Brito, J., Lee, J. D., and Coe, H.: Airborne observations of IEPOX-derived isoprene SOA in the Amazon during SAMBBA, *Atmospheric Chemistry and Physics*, 14, 11 393–11 407, doi:10.5194/acp-14-11393-2014, <http://www.atmos-chem-phys.net/14/11393/2014/>, 2014.
- Artaxo, A., Rizzo, L. V., Brito, J. F., Barbosa, H. M. J., Arana, A., Sena, E. T., Cirino, G. G., Bastos, W., Martin, S. T., and Andreae, M. O.: Atmospheric Aerosols in Amazonia and Land Use Change: From Natural Biogenic to Biomass Burning Conditions, *Faraday Discussions*, 165, 2013.
- Bellouin, N., Rae, J., Jones, A., Johnson, C., Haywood, J., and Boucher, O.: Aerosol forcing in the Climate Model Intercomparison Project (CMIP5) simulations by HadGEM2-ES and the role of ammonium nitrate, *Journal of Geophysical Research*, 116, doi:10.1029/2011jd016074, 2011.
- Brem, B. T., Gonzalez, F. C. M., Meyers, S. R., Bond, T. C., and Rood, M. J.: Laboratory-Measured Optical Properties of Inorganic and Organic Aerosols at Relative Humidities up to 95doi:10.1080/02786826.2011.617794, <GotoISI>://WOS:000297065900006, 848PZ Times Cited:11 Cited References Count:49, 2012.
- Brilo, J., Rizzo, L. V., Morgan, W. T., Coe, H., Johnson, B., Haywood, J., Longo, K., Freitas, S., Andreae, M. O., and Artaxo, P.: Ground-based aerosol characterization during the South American Biomass Burning Analysis (SAMBBA) field experiment, *Atmospheric Chemistry and Physics*, 14, 12 069–12 083, doi:10.5194/acp-14-12069-2014, <http://www.atmos-chem-phys.net/14/12069/2014/>, 2014.
- Charlson, R. J., Schwartz, S. E., Hales, J. M., Cess, R. D., Coakley, J. A., Hansen, J. E., and Hofmann, D. J.: Climate Forcing by Anthropogenic Aerosols, *Science*, 255, 423–430, doi:10.1126/science.255.5043.423, <http://science.sciencemag.org/content/255/5043/423>, 1992.
- Collini, E. A., Berbery, E. H., Barros, V. R., and Pyle, M. E.: How Does Soil Moisture Influence the Early Stages of the South American Monsoon?, *Journal of Climate*, 21, 195–213, doi:10.1175/2007JCLI1846.1, <https://doi.org/10.1175/2007JCLI1846.1>, 2008.
- Darbyshire, E., T., M. W., Allan, J., Liu, D., Flynn, M., Dorsey, J., O'Shea, S., Trembath, J., Johnson, B., Szpek, K., Marengo, F., Haywood, J., Brito, J., Artaxo, P., Longo, K., and Coe, H.: Contrasting aerosol heating from biomass burning haze between deforestation and Cerrado regions of tropical South America, as derived from airborne composition measurements, In prep., 2017.
- DeFries, R. S., Morton, D. C., van der Werf, G. R., Giglio, L., Collatz, G. J., Randerson, J. T., Houghton, R. A., Kasibhatla, P. K., and Shimabukuro, Y.: Fire-related carbon emissions from land use transitions in southern Amazonia, *Geophysical Research Letters*, 35, doi:10.1029/2008GL035689, <http://www.escholarship.org/uc/item/06s5w3t5>, 2008.
- Garreaud, R. D., Vuille, M., Compagnucci, R., and Marengo, J.: Present-day South American climate, *Palaeogeography, Palaeoclimatology, Palaeoecology*, 281, 180 – 195, doi:http://dx.doi.org/10.1016/j.palaeo.2007.10.032, <http://www.sciencedirect.com/science/article/pii/S0031018208005002>, long-term multi-proxy climate reconstructions and dynamics in South America (LOTRED-SA): State of the art and perspectives, 2009.



- Gonçalves, W. A., Machado, L. A. T., and Kirstetter, P.-E.: Influence of biomass aerosol on precipitation over the Central Amazon: an observational study, *Atmospheric Chemistry and Physics*, 15, 6789–6800, doi:10.5194/acp-15-6789-2015, <https://www.atmos-chem-phys.net/15/6789/2015/>, 2015.
- Hansen, J., Sato, M., and Ruedy, R.: Radiative forcing and climate response, *Journal of Geophysical Research: Atmospheres*, 102, 6831–6864, doi:10.1029/96JD03436, <http://dx.doi.org/10.1029/96JD03436>, 1997.
- Haywood, J. M., Allan, R. P., Culverwell, I., and Slingo, T.: Can desert dust explain the anomalous greenhouse effect observed over the Sahara during July 2003 revealed by GERB/UM intercomparisons?, Report, 2003.
- Hewitt, H. T., Copsey, D., Culverwell, I. D., Harris, C. M., Hill, R. S. R., Keen, A. B., McLaren, A. J., and Hunke, E. C.: Design and implementation of the infrastructure of HadGEM3: the next-generation Met Office climate modelling system, *Geoscientific Model Development*, 4, 223–253, doi:10.5194/gmd-4-223-2011, <http://www.geosci-model-dev.net/4/223/2011/>, 2011.
- Hodgson, A. K., Morgan, W. T., O’Shea, S., Bauguitte, S., Allan, J. D., Darbyshire, E., Flynn, M. J., Liu, D., Lee, J., Johnson, B., Haywood, J., Longo, K. M., Artaxo, P. E., and Coe, H.: Near-field emission profiling of Rainforest and Cerrado fires in Brazil during SAMBBA 2012, *Atmospheric Chemistry and Physics Discussions*, 2017, 1–33, doi:10.5194/acp-2016-1019, <http://www.atmos-chem-phys-discuss.net/acp-2016-1019/>, 2017.
- Jiang, H. and Feingold, G.: Effect of aerosol on warm convective clouds: Aerosol-cloud-surface flux feedbacks in a new coupled large eddy model, *Journal of Geophysical Research: Atmospheres*, 111, n/a–n/a, doi:10.1029/2005JD006138, <http://dx.doi.org/10.1029/2005JD006138>, d01202, 2006.
- Johnson, B. T., Shine, K. P., and Forster, P. M.: The semi-direct aerosol effect: Impact of absorbing aerosols on marine stratocumulus, *Quarterly Journal of the Royal Meteorological Society*, 130, 1407–1422, doi:10.1256/qj.03.61, <http://dx.doi.org/10.1256/qj.03.61>, 2004.
- Johnson, B. T., Haywood, J. M., Langridge, J. M., Darbyshire, E., Morgan, W. T., Szpek, K., Brooke, J. K., Marengo, F., Coe, H., Artaxo, P., Longo, K. M., Mulcahy, J. P., Mann, G. W., Dalvi, M., and Bellouin, N.: Evaluation of biomass burning aerosols in the HadGEM3 climate model with observations from the SAMBBA field campaign, *Atmospheric Chemistry and Physics*, 16, 14 657–14 685, doi:10.5194/acp-16-14657-2016, <http://www.atmos-chem-phys.net/16/14657/2016/>, 2016.
- Jones, A., Bellouin, N., and Haywood, J. M.: Improvements to the Biomass-burning Aerosol Scheme for the HadGEM1a Model, Report, DEFRA, 2005.
- Koch, D. and Del Genio, A. D.: Black carbon semi-direct effects on cloud cover: review and synthesis, *Atmospheric Chemistry and Physics*, 10, 7685–7696, doi:10.5194/acp-10-7685-2010, 2010.
- Koren, I., Kaufman, Y. J., Remer, L. A., and Martins, J. V.: Measurement of the Effect of Amazon Smoke on Inhibition of Cloud Formation, *Science*, 303, 1342–1345, doi:10.1126/science.1089424, <http://science.sciencemag.org/content/303/5662/1342>, 2004.
- Koren, I., Martins, J. V., Remer, L. A., and Afargan, H.: Smoke Invigoration Versus Inhibition of Clouds over the Amazon, *Science*, 321, 946–949, doi:10.1126/science.1159185, <http://science.sciencemag.org/content/sci/321/5891/946.full.pdf>, 2008.
- Kotchenruther, R. A. and Hobbs, P. V.: Humidification factors of aerosols from biomass burning in Brazil, *Journal of Geophysical Research: Atmospheres*, 103, 32 081–32 089, doi:10.1029/98jd00340, 1998.
- Lamarque, J.-F., Bond, T. C., Eyring, V., Granier, C., Heil, A., Klimont, Z., Lee, D., Liousse, C., Mieville, A., Owen, B., Schultz, M. G., Shindell, D., Smith, S. J., Stehfest, E., Van Aardenne, J., Cooper, O. R., Kainuma, M., Mahowald, N., McConnell, J. R., Naik, V., Riahi, K., and van Vuuren, D. P.: Historical (1850–2000) gridded anthropogenic and biomass burning emissions of reactive gases and aerosols: methodology and application, *Atmospheric Chemistry and Physics*, 10, 7017–7039, doi:10.5194/acp-10-7017-2010, <http://www.atmos-chem-phys.net/10/7017/2010/>, 2010.



- Liebmann, B. and Marengo, J.: Interannual Variability of the Rainy Season and Rainfall in the Brazilian Amazon Basin, *Journal of Climate*, 14, 4308–4318, doi:10.1175/1520-0442(2001)014<4308:IVOTRS>2.0.CO;2, [https://doi.org/10.1175/1520-0442\(2001\)014<4308:IVOTRS>2.0.CO;2](https://doi.org/10.1175/1520-0442(2001)014<4308:IVOTRS>2.0.CO;2), 2001.
- Liebmann, B. and Mechoso, C. R.: *The South American Monsoon System*, World Scientific, 2011.
- 5 Magi, B. I. and Hobbs, P. V.: Effects of humidity on aerosols in southern Africa during the biomass burning season, *Journal of Geophysical Research: Atmospheres*, 108, n/a–n/a, doi:10.1029/2002jd002144, 2003.
- Marengo, F., Johnson, B., Langridge, J. M., Mulcahy, J., Benedetti, A., Remy, S., Jones, L., Szpek, K., Haywood, J., Longo, K., and Artaxo, P.: On the vertical distribution of smoke in the Amazonian atmosphere during the dry season, *Atmospheric Chemistry and Physics*, 16, 2155–2174, doi:10.5194/acp-16-2155-2016, <http://www.atmos-chem-phys.net/16/2155/2016/>, 2016.
- 10 Marengo, J. A., Liebmann, B., Kousky, V. E., Filizola, N. P., and Wainer, I. C.: Onset and End of the Rainy Season in the Brazilian Amazon Basin, *Journal of Climate*, 14, 833–852, doi:doi:10.1175/1520-0442(2001)014<0833:OAEOTR>2.0.CO;2, <http://journals.ametsoc.org/doi/abs/10.1175/1520-0442%282001%29014%3C0833%3AOAEOTR%3E2.0.CO%3B2>, 2001.
- Marengo, J. A., Liebmann, B., Grimm, A. M., Misra, V., Dias, P. L. S., F., I., Cavalcanti, A., Carvalho, L. M. V., Berbery, E. H., Ambrizzi, T., Vera, C. S., Saulo, A. C., Nogués-Paegle, J., Zipser, E., Seth, A., and Alves, L. M.: Recent developments on the South American monsoon system, *International Journal of Climatology*, 32, 1–21, doi:10.1002/joc2254, 2012.
- 15 Raia, A. and Cavalcanti, I. F. A.: The Life Cycle of the South American Monsoon System, *Journal of Climate*, 21, 6227–6246, doi:doi:10.1175/2008JCLI2249.1, <http://journals.ametsoc.org/doi/abs/10.1175/2008JCLI2249.1>, 2008.
- Rap, A., Spracklen, D. V., Mercado, L., Reddington, C. L., Haywood, J. M., Ellis, R. J., Phillips, O. L., Artaxo, P., Bonal, D., Restrepo Coupe, N., and Butt, N.: Fires increase Amazon forest productivity through increases in diffuse radiation, *Geophysical Research Letters*, 42, 4654–4662, doi:10.1002/2015GL063719, <http://dx.doi.org/10.1002/2015GL063719>, 2015GL063719, 2015.
- 20 Rayner, N. A., Parker, D. E., Horton, E. B., Folland, C. K., Alexander, L. V., Rowell, D. P., Kent, E. C., and Kaplan, A.: Global analyses of sea surface temperature, sea ice, and night marine air temperature since the late nineteenth century, *Journal of Geophysical Research: Atmospheres*, 108, n/a–n/a, doi:10.1029/2002JD002670, <http://dx.doi.org/10.1029/2002JD002670>, 4407, 2003.
- Reddington, C. L., Butt, E. W., Ridley, D. A., Artaxo, P., Morgan, W. T., Coe, H., and Spracklen, D. V.: Air quality and human health improvements from reductions in deforestation-related fire in Brazil, *Nature Geoscience*, 8, 768–771, doi:10.1038/ngeo2535, 2015.
- Rosenfeld, D.: Suppression of Rain and Snow by Urban and Industrial Air Pollution, *Science*, 287, 1793–1796, doi:10.1126/science.287.5459.1793, <http://science.sciencemag.org/content/287/5459/1793>, 2000.
- Sena, E. T., Artaxo, P., and Correia, A. L.: Spatial variability of the direct radiative forcing of biomass burning aerosols and the effects of land use change in Amazonia, *Atmospheric Chemistry and Physics*, 13, 1261–1275, doi:10.5194/acp-13-1261-2013, <http://www.atmos-chem-phys.net/13/1261/2013/>, 2013.
- 30 Spracklen, D. V., Carslaw, K. S., Pöschl, U., Rap, A., and Forster, P. M.: Global cloud condensation nuclei influenced by carbonaceous combustion aerosol, *Atmos. Chem. Phys.*, 11, 9067–9087, doi:10.5194/acp-11-9067-2011, <http://www.atmos-chem-phys.net/11/9067/2011/>, 2011.
- Ten Hoeve, J. E., Jacobson, M. Z., and Remer, L. A.: Comparing results from a physical model with satellite and in situ observations to determine whether biomass burning aerosols over the Amazon brighten or burn off clouds, *Journal of Geophysical Research. Atmospheres*, 117, doi:10.1175/1520-0469(1957)014h0272:AEIOTEi2.0.CO;2g, copyright - Copyright 2012 by the American Geophysical Union, 2012.
- Twomey, S.: Pollution and the planetary albedo, *Atmospheric Environment*, 8, 1251–1256, doi:[https://doi.org/10.1016/0004-6981\(74\)90004-3](https://doi.org/10.1016/0004-6981(74)90004-3), <http://www.sciencedirect.com/science/article/pii/0004698174900043>, 1974.



- Twomey, S.: The Influence of Pollution on the Shortwave Albedo of Clouds, *Journal of the Atmospheric Sciences*, 34, 1149–1152, doi:10.1175/1520-0469(1977)034<1149:TIOPOT>2.0.CO;2, [https://doi.org/10.1175/1520-0469\(1977\)034<1149:TIOPOT>2.0.CO;2](https://doi.org/10.1175/1520-0469(1977)034<1149:TIOPOT>2.0.CO;2), 1977.
- van der Werf, G. R., Randerson, J. T., Giglio, L., Collatz, G. J., Mu, M., Kasibhatla, P. S., Morton, D. C., DeFries, R. S., Jin, Y., and van Leeuwen, T. T.: Global fire emissions and the contribution of deforestation, savanna, forest, agricultural, and peat fires (1997–2009), *Atmospheric Chemistry and Physics*, 10, 11707–11735, doi:10.5194/acp-10-11707-2010, <http://www.atmos-chem-phys.net/10/11707/2010/>, 2010.
- Vera, C., Higgins, W., Amador, J., Ambrizzi, T., Garreaud, R., Gochis, D., Gutzler, D., Lettenmaier, D., Marengo, J., Mechoso, C. R., Nogues-Paegle, J., Dias, P. L. S., and Zhang, C.: Toward a Unified View of the American Monsoon Systems, *Journal of Climate*, 19, 4977–5000, doi:10.1175/JCLI3896.1, <https://doi.org/10.1175/JCLI3896.1>, 2006.
- Warner, J.: A Reduction in Rainfall Associated with Smoke from Sugar-Cane Fires - An Inadvertent Weather Modification?, *Journal of Applied Meteorology*, 7, 247–251, doi:10.1175/1520-0450(1968)007<0247:ARIRAW>2.0.CO;2, [https://doi.org/10.1175/1520-0450\(1968\)007<0247:ARIRAW>2.0.CO;2](https://doi.org/10.1175/1520-0450(1968)007<0247:ARIRAW>2.0.CO;2), 1968.
- Wilson, D. R., Bushell, A. C., Kerr-Munslow, A. M., Price, J. D., and Morcrette, C. J.: PC2: A prognostic cloud fraction and condensation scheme. I: Scheme description, *Quarterly Journal of the Royal Meteorological Society*, 134, 2093–2107, doi:10.1002/qj.333, <http://dx.doi.org/10.1002/qj.333>, 2008a.
- Wilson, D. R., Bushell, A. C., Kerr-Munslow, A. M., Price, J. D., Morcrette, C. J., and Bodas-Salcedo, A.: PC2: A prognostic cloud fraction and condensation scheme. II: Climate model simulations, *Quarterly Journal of the Royal Meteorological Society*, 134, 2109–2125, doi:10.1002/qj.332, <http://dx.doi.org/10.1002/qj.332>, 2008b.
- Zhang, Y., Fu, R., Yu, H., Dickinson, R. E., Juarez, R. N., Chin, M., and Wang, H.: A regional climate model study of how biomass burning aerosol impacts land-atmosphere interactions over the Amazon, *Journal of Geophysical Research: Atmospheres*, 113, doi:10.1029/2007JD009449, <http://dx.doi.org/10.1029/2007JD009449>, d14S15, 2008.
- Zhang, Y., Fu, R., Yu, H., Qian, Y., Dickinson, R., Silva Dias, M. A. F., da Silva Dias, P. L., and Fernandes, K.: Impact of biomass burning aerosol on the monsoon circulation transition over Amazonia, *Geophysical Research Letters*, 36, doi:10.1029/2009GL037180, <http://dx.doi.org/10.1029/2009GL037180>, 2009.
- Zou, J., Sun, J., Ding, A., Wang, M., Guo, W., and Fu, C.: Observation-based estimation of aerosol-induced reduction of planetary boundary layer height, *Advances in Atmospheric Sciences*, 34, 1057–1068, doi:10.1007/s00376-016-6259-8, <https://doi.org/10.1007/s00376-016-6259-8>, 2017.